An investigation of the damping properties of Vacrosil-010

O'Toole, John Francis, Jr.

NAVAL POSTGRADUATE SCHOOL
Monterey, California

THESIS

AN INVESTIGATION OF THE DAMPING PROPERTIES OF VACROSIL-010

by

John Francis O'Toole, Jr.

December 1986

Thesis Advisor: A.J. Perkins

Approved for Public Release; distribution is unlimited

REPORT DOCUMENTATION PAGE

1a REPORT SECURITY CLASSIFICATION UNCLASSIFIED	1b RESTRICTIVE MARKINGS
2a SECURITY CLASSIFICATION AUTHORITY	3 DISTRIBUTION/AVAILABILITY OF REPORT Approved for Public Release; Distribution is unlimited.
2b DECLASSIFICATION/DOWNGRADING SCHEDULE	
4 PERFORMING ORGANIZATION REPORT NUMBER(S)	5 MONITORING ORGANIZATION REPORT NUMBER(S)
6a NAME OF PERFORMING ORGANIZATION Naval Postgraduate School 6b OFFICE SYMBOL (If applicable) 69	7a NAME OF MONITORING ORGANIZATION Naval Postgraduate School
6c ADDRESS (City, State, and ZIP Code) Monterey, California 93943-5000	7b ADDRESS (City, State, and ZIP Code) Monterey, California 93943-5000
8a NAME OF FUNDING/SPONSORING ORGANIZATION 8b OFFICE SYMBOL (If applicable)	9 PROCUREMENT INSTRUMENT IDENTIFICATION NUMBER
8c ADDRESS (City, State, and ZIP Code)	10 SOURCE OF FUNDING NUMBERS PROGRAM ELEMENT NO / PROJECT NO / TASK NO / WORK UNIT ACCESSION NO

11 TITLE (Include Security Classification)
AN INVESTIGATION OF THE DAMPING PROPERTIES OF VACROSIL-010

12 PERSONAL AUTHOR(S)
O'Toole, John Francis, Jr.

13a TYPE OF REPORT	13b TIME COVERED	14 DATE OF REPORT (Year, Month, Day)	15 PAGE COUNT
Master's Thesis	FROM _____ TO _____	1986 December	92

16 SUPPLEMENTARY NOTATION

17 COSATI CODES			18 SUBJECT TERMS (Continue on reverse if necessary and identify by block number)
FIELD	GROUP	SUB-GROUP	Strain-Dependent Damping, Vacrosil-010, Microstructure, Resonant Dwell Technique, Specific Damping Capacity (SDC), Forced Vibrations, Iron-Chromium-Molybdenum (Fe-Cr-Mo)

19 ABSTRACT (Continue on reverse if necessary and identify by block number)

The strain dependence and specific damping capacity (SDC) of the damping alloy, Vacrosil-010 (84.5 Fe, 11.3 Cr, 2.4 Mo), was determined using a modified version of the resonant dwell technique. Cantilever beam specimens were annealed for 1 hour at temperatures between 800°C and 1100°C. They were subsequently vibrated at their first three resonant modes (0-1000Hz) at room temperature.

The effect on damping capacity of changes in heat treatment were investigated using tensile hysteresis testing, optical microscopy, X-ray diffraction (XRD), and scanning electron microscopy (SEM).

20 DISTRIBUTION/AVAILABILITY OF ABSTRACT ☒ UNCLASSIFIED/UNLIMITED ☐ SAME AS RPT ☐ DTIC USERS	21 ABSTRACT SECURITY CLASSIFICATION UNCLASSIFIED
22a NAME OF RESPONSIBLE INDIVIDUAL A.J. Perkins	22b TELEPHONE (Include Area Code) (408) 646-2216 22c OFFICE SYMBOL 69Ps

DD FORM 1473, 84 MAR 83 APR edition may be used until exhausted
All other editions are obsolete

Approved for public release; distribution is unlimited

An Investigation of the Damping Properties of VACROSIL-010

by

John Francis O'Toole, Jr.
Lieutenant, United States Navy
B.S., Georgia Institute of Technology, 1980

Submitted in partial fulfillment of the requirements for the degree of

MASTER OF SCIENCE IN MECHANICAL ENGINEERING

from the

NAVAL POSTGRADUATE SCHOOL
December 1986

ABSTRACT

The strain dependence and specific damping capacity (SDC) of the damping alloy, VACROSIL-010 (84.5 Fe, 11.3 Cr, 2.4 Mo), was determined using a modified version of the resonant dwell technique. Cantilever beam specimens were annealed for 1 hour at temperatures between 800°C and 1100°C. They were subsequently vibrated at their first three resonant modes (0-1000Hz) at room temperature.

The effect on damping capacity of changes in heat treatment were investigated using tensile hysteresis testing, optical microscopy, X-ray diffraction (XRD), and scanning electron microscopy (SEM).

TABLE OF CONTENTS

LIST OF TABLES

LIST OF FIGURES

DEDICATION

To my wife, Anita, whose patience and support made a difficult project a more pleasant experience than it might have been.

ACKNOWLEDGEMENT

I would like to thank my advisor, Professor A. J. Perkins, for his guidance in the conduct of this research. I would further like to acknowledge the assistance and instruction given me by Dr. S. J. Hales, Tom Kellogg, and Tammy Ellis.

I. INTRODUCTION

A. GENERAL

Noise abatement and vibration control of dynamic systems (e.g., propulsion systems) are highly desirable features currently under investigation by the Navy for application in submarine and surface ship design. Conventional structural alloys generally do not exhibit significant damping at stress amplitudes associated with vibration and noise emission. Therefore, as outlined by Schetky and Perkins [Ref. 1], there are three principle methods of vibration and noise control which are employed: 1. Isolation of the source of vibration and noise (i.e., moving parts) and the surfaces to which they radiate energy. 2. Dissipation and attenuation of energies generated within the structure through the use of absorbing pads (i.e., rubber insulation for pipe hangers, resilient mounts). 3. Attenuation of vibration and noise through the use of materials whose composition and microstructure combine to absorb energy internally and dissipate it.

The first two methods are effective, but in achieving their design goals, they contribute significant additional weight and utilize valuable space, features which tend to make them undesirable in applications aboard submarines and ships. The third method has the potential

to eliminate these problems, since there is the possibility of having a design without cumbersome attachments or encapsulated structures. However, the alloy design of high damping materials which fulfill the structural and energy-absorption functions of machine parts and construction materials is very difficult.

In general, there are two primary problems associated with designing a material with high damping characteristics [Ref. 2:p. 1].

1. Problems in the development of reliable methods for accurate measurement of the energy conversion process occuring within the material.

2. A need to understand the fundamental processes involved in the energy transfer occuring within the material (i.e., the damping mechanisms) and how these mechanisms relate to the microstructure.

Current research by the Navy on the use of materials with high internal damping mechanisms is directed toward the investigation of the specific damping capacities of existing commercial alloys and the relationships between the mechanisms of damping and microstructure and physical properties. The ultimate extension of this research will hopefully result in the development of alloys designed with optimum damping and structural characteristics.

B. BACKGROUND

All materials exhibit some degree of vibrational damping through energy absorbing or energy dissipative phenomena. As mentioned previously, most structural alloys

exhibit poor damping capacity at the amplitudes of stress associated with vibration and noise emission. The specific damping capacities of the more common structural alloys (steel, brasses, aluminum alloys) are less than 1% (see Table 1). Cast products, such as gray cast iron, typically show higher capacities for damping than wrought. The internal mechanism of gray cast iron which contributes to vibration damping is related to the large, flake-like particles of graphite in the microstructure, which are effective in absorbing energy resulting in specific damping capacities ranging from 5% to 10% [Ref.1:p. 203]. However, other types of cast iron, containing more rounded graphite particles within the microstructure, exhibit lower damping capacities.

In recent years, several new alloys have been developed which exhibit significantly higher specific damping capacities (in excess of 40%), including Cu-Mn-based alloys (SONOSTON, INCRAMUTE), Ni-Ti alloys (NITINOL), and Fe-Cr-based alloys (SILENTALLOY, VACROSIL, GENTALOY, etc.) Damping in these high damping alloys, as in any material, traces its origin to microstructural effects and interactions, as the microstructure of a material largely determines the mechanism(s) responsible for damping when given external variables are imposed. As outlined by de Batist [Ref.3], some external variables (such as frequency, strain amplitude and number of cycles) have a direct

relation with the vibrational state. In the area of high damping phenomena, the external variables can produce a variety of microstructural responses, which in general result in damping due to irreversibilities incurred when a material is subjected to an alternating stress. This results in the absorption of energy via "internal friction" due to these irreversibilities. The internal friction results in the energy loss per cycle which is referred to as damping. The energy losses which characterize these irreversibilities may be evident in hysteresis curves representing magnetic, mechanical, and/or thermal losses. The degree of energy loss is closely tied to changes in the microstructure as a function of:

- composition of the constituents within an alloy system
- thermomechanical history
- operating above or below a specific threshold temperature
- operating above or below a particular stress level

As a crystalline material is cyclically stressed, several microstructural damping mechanisms may be activated. They are:

- dislocation damping [Refs. 3,4]
- interphase boundary damping [Ref. 3]
- phase change effects [Ref. 3]

TABLE 1

DAMPING CHARACTERISTICS OF SELECTED METALS AT ROOM TEMPERATURE [REF. 1]

METAL	SDC (%)	YIELD STRENGTH (10^3 PSI)	DENSITY (gm/cm^3)
Magnesium (wrought)	49	26	1.74
Cu-Mn alloys (INCRAMUTE, SONOSTON)	40	45	7.5
Ni-Ti alloy	40	25	6.45
Fe-Cr-Al alloy	40	40	7.4
High-C gray iron	19	25	7.7
Nickel (pure)	18	9	8.9
Iron (pure)	16	10	7.86
Martensitic stainless steel	8	85	7.7
Gray cast iron	6	25	7.8
SAP (aluminum powder)	5	20	2.55
Low-carbon steel	4	50	7.86
Ferritic stainless steel	3	45	7.75
Malleable, nodular cast irons	2	50	7.8
Medium-carbon steel	1	60	7.866
Austenitic stainless steel	1	35	7.8
1100 Aluminum	0.3	5	2.71
Aluminum alloy 2024-T4	<0.2	47	2.77
Nickel-base superalloys	<0.2	RANGE	8.5
Titanium alloys	<0.2	RANGE	4.5
Brasses, bronzes	<0.2	RANGE	8.5

Previous research on "quiet alloys" at the Naval Postgraduate School has been concerned mainly with nonferrous alloys, specifically the Cu-Mn based alloys, SONOSTON [Ref. 5] and INCRAMUTE [Ref. 6], whose mechanism for damping apparently involve the interaction of cyclic stress twinned and "tweed" microstructures (interphase boundary damping).

In our study, the area of interest concerns itself with iron-chromium (Fe-Cr)-based alloys, and specifically

an iron-chromium-molybdenum (Fe-Cr-Mo) alloy commercially known as VACROSIL-010. Previous research by Cochardt [Ref. 7], de Batist [Ref. 3], Schilling and Houze [Ref. 8], Willertz [Ref. 9], Suzuki, et al. [Ref. 10], Masumoto, et al. [Refs. 11-13], Schneider, et al. [Ref. 14], and Kasper [Ref. 15] has established that the primary damping mechanism for this alloy group is a function of the ferromagnetic properties of the material. According to de Batist [Ref. 3:p. 43], the damping is intimately related to the magnetomechanical interaction phenomena which naturally occurs in a ferromagnetic material (domain boundary damping).

C. OBJECTIVE

High material damping in various ferrous alloys, especially the binary systems Fe-Cr (12-16 wt. % Cr) [Ref. 11] and Fe-Mo (2-5 wt % Mo) [Ref. 12], has been previously reported, as well as in the ternary Fe-Mo-Cr [Refs. 10,13] and Fe-Cr-Al [Refs.16-19] systems. A relatively new high damping Fe-Cr-based alloy has beed introduced to the commercial market by Vacuumschmelze, G.M.B.H. (VAC), of Hanau, West Germany, with the registered trade name of VACROSIL-010. This material is available in two diverse compositions (Fe-Cr-Al and Fe-Cr-Mo, the latter refered to as a corrosion resistant grade) [Ref.15]. The corrosion resistant version of VACROSIL-010 (Fe-Cr-Mo, which will be refered to here as VACROSIL-010(Mo)) is of especial

interest to the Navy. Bearing this in mind, the following objectives guided this research:

- to determine the relationship between the room temperature damping properties of VACROSIL-010(Mo) to applied strain (or stress) under random vibration conditions for various heat treatment conditions (1 hour annealing at various temperatures between 800°C and 1100°C followed by subsequent furnace cooling or water quench).
- to attempt to metallographically characterize the microstructures associated with high damping in VACROSIL-010 (Mo).
- to survey the physical properties of the material for various heat treated conditions and determine their relationship with damping.

D. MACROSTRUCTURAL DAMPING

1. Measurement of Damping

The ability of a material to absorb vibrational energy and transfer that energy to other forms is defined as the damping capacity of a solid. The specific damping capacity is the fraction of the vibrational energy or amplitude absorbed during one cycle of vibration. There are several parameters which characterize the vibration damping of a material.

a. Logarithmic Decrement (δ)

The natural logarithm of the ratio of any two successive amplitudes is the logarithmic decrement. For a linear system, free vibrations decay exponentially. Therefore, the faster the decay, the larger the damping. [Ref. 20:p. 138]

$$\delta = \ln(a_i/a_{i+1}) = (1/n)\ln(a_o/a_n) \qquad \text{(eqn 1.1)}$$

where n = number of cycles between a_o and a_n

b. Quality Factor (Q)

A measurement of the sharpness of a resonance peak is known as the quality factor. [Ref. 21:p. 76]

$$Q = \omega_n/\omega_2-\omega_1 = 1/2\zeta \qquad \text{(eqn 1.2)}$$

where ζ = damping factor

c. Internal Friction (Q^{-1})

The inverse of the quality factor is known as internal friction. [Ref. 3:p. 41]

$$Q^{-1} = (\omega_2-\omega_1)/\omega_n = 2\zeta \qquad \text{(eqn 1.3)}$$

This is also known as the loss factor which is defined as the ratio of the loss modulus and the dynamic elasticity or storage modulus.

d. Normalized Bandwith

For the half power point method: damping can be measured in terms of the width ($\omega_2-\omega_1$) of the peak at the resonant frequency (ω_n) at points corresponding to .707 of the amplitude. This corresponds to the points at which the stored energy is half its maximum value at the resonant frequency and normalized by the associated resonant frequency. [Ref. 19:p. 76]

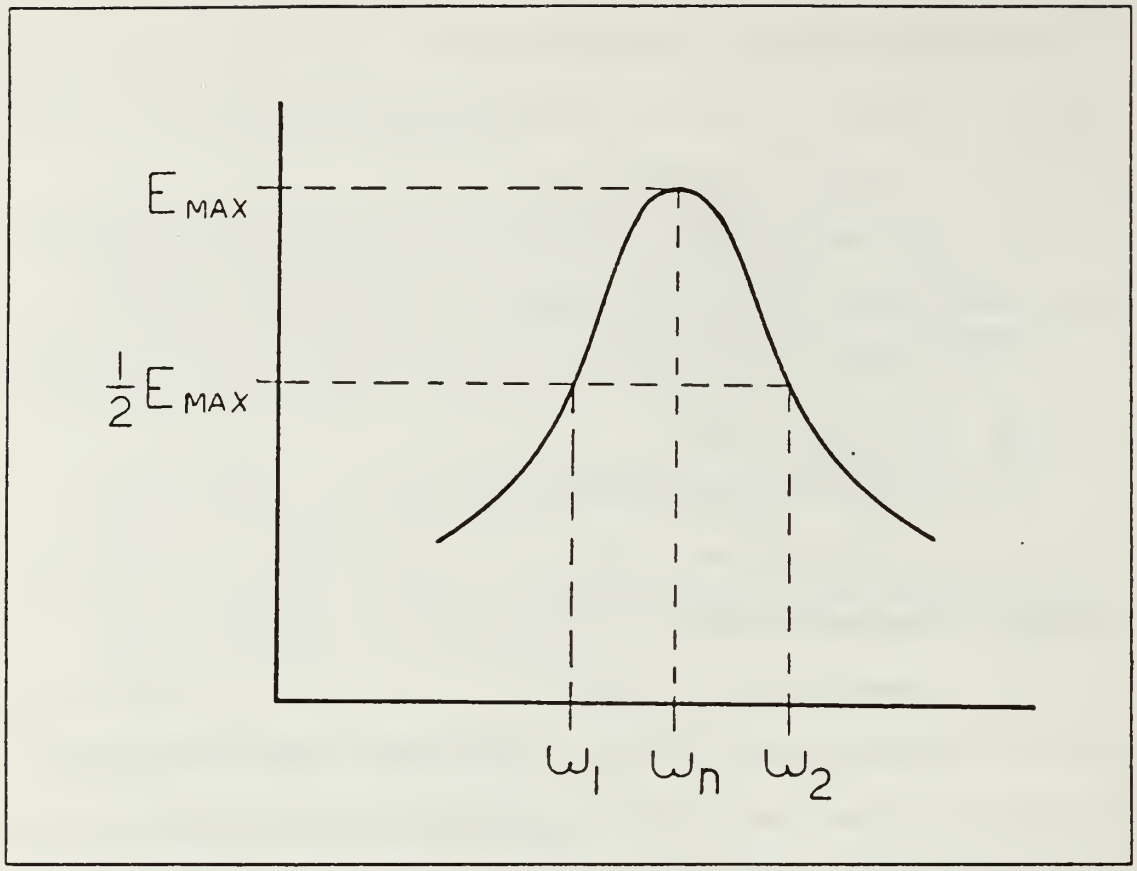

Figure 1.1 Normalized Bandwith [Ref. 15:p. 17]

e. Specific Damping Capacity (SDC)

The SDC is the percentage of strain energy dissipated during a stress cycle for an oscillating system [Ref. 22:p. 444].

$$SDC = (a_{i+1}^2 - a_i^2)/a_i^2 \qquad \text{(eqn 1.4)}$$

if $(a_{i+1}-a_i)$ is small, SDC can be approximated by [Ref. 22:p. 444]

$$SDC = 2(a_{i+1}-a_i)/a_i \qquad \text{(eqn 1.5)}$$

f. Phase Angle (α)

The angle by which strain lags behind stress under cyclic loading is known as the phase angle. [Ref. 22:p. 445]

$$\tan \alpha = (1/\pi)\ln(a_i/a_{i+1}) = \delta/\pi \qquad \text{(eqn 1.6)}$$

For small values of damping, ($\zeta << 0.5$) the following relations hold: [Ref. 6:p. 18-19]

$$\tan \alpha = \delta/\pi = Q^{-1} = 2\zeta$$

$$SDC(\%) = 200\pi Q^{-1} \qquad \text{(eqn 1.7)}$$

g. Resonant Frequency (ω_n)

The natural frequency of a cantilever beam corresponding to the n^{th} mode [Ref. 21:p. 464]

$$\omega_n = (\beta_n l)^2 (EI/ml^4)^{1/2} \qquad \text{(eqn 1.8)}$$

where

E Young's Modulus of Elasticity

I Moment of Inertia

m mass density per unit length

l vibrating length of beam

$\beta_n l$ function of the mode of vibration of the beam values for several different modes (n) are given below for a clamped-free beam [Ref. 21:p. 466]

n	$\beta_n l$	$(\beta_n l)^2$
1	1.8751	3.5160
2	4.6941	22.0345
3	7.8548	61.6972

2. Macrostructural Damping Techniques

Damping measurements on Fe-Cr alloys have been performed in most cases in the past using either an inverted torsion pendulum apparatus [Refs. 11-13,17] under free decay conditions, or via forced vibration [Ref. 9]. Another method which has been utilized has been the cantilever beam method [Ref. 10,14] where damping is also determined from the decay of free oscillations.

A method which has begun to enjoy increasing popularity is the single cantilever beam resonance dwell apparatus. This method, developed by Bolt, Beranek and Newman, Inc. [Ref. 23] can be used to determine the stress and frequency dependence of material damping over a 25-1000 Hz frequency range. The resonance dwell technique is a forced vibration method of indirectly determining the loss factor of a simple structural element by measuring its response to excitation at a modal frequency. This method was demonstrated successfully as an effective means of vibration damping measurement for high damping alloys by Kaufman, Kulin, and Neshe [Ref. 24] for NiTi and CuAlNi.

The structural element used is a cantilever beam which is clamped to a bar, which in turn is connected at one end to an electromagnetic shaker and the other end to a heavy base. An accelerometer is mounted to the bar at the root of the sample. The response of the support system is measured in this way. The specimen (cantilever beam)

response is measured by means of a microscope focused on the tip of the cantilever beam. The tip is illuminated by a stroboscope set to flash at nearly the same frequency as the mechanical oscillation of the tip of the beam. The fundamental natural frequency, f, of a cantilever beam of length L (inches) and thickness h (inches) is: [Ref. 23:p. 6]

$$f = (1/2\pi)(C_n/L)^2 h(32E/\rho)^{1/2} \text{ (cycles/sec)} \quad \text{(eqn 1.9)}$$

where $C_n = \beta_n l$ from (eqn 1.8) and ρ is the density of the sample in (lb/in^3) and E is the dynamic Young's Modulus. The length is the vibrating length of the beam, while the width is 0.5 inches, conforming to the width of the bar to which the specimens are clamped (see Figure 1.2).

A modified version of this method was developed by Professor Y. S. Shin of the Naval Postgraduate School. In this, the optical microscope assembly is replaced by an accelerometer mounted at the beam tip. The signals produced by the input accelerometer (at the root of the specimen) and the output accelerometer (at the tip) are processed by a spectrum analyzer to produce the frequency response of the vibrating beam at a resonant mode. This method has been tested and compared to a forced torsion pendulum device for the measurement of damping in SONOSTON by Dew [Ref. 5] and further tested by Reskusich [Ref. 6] for INCRAMUTE.

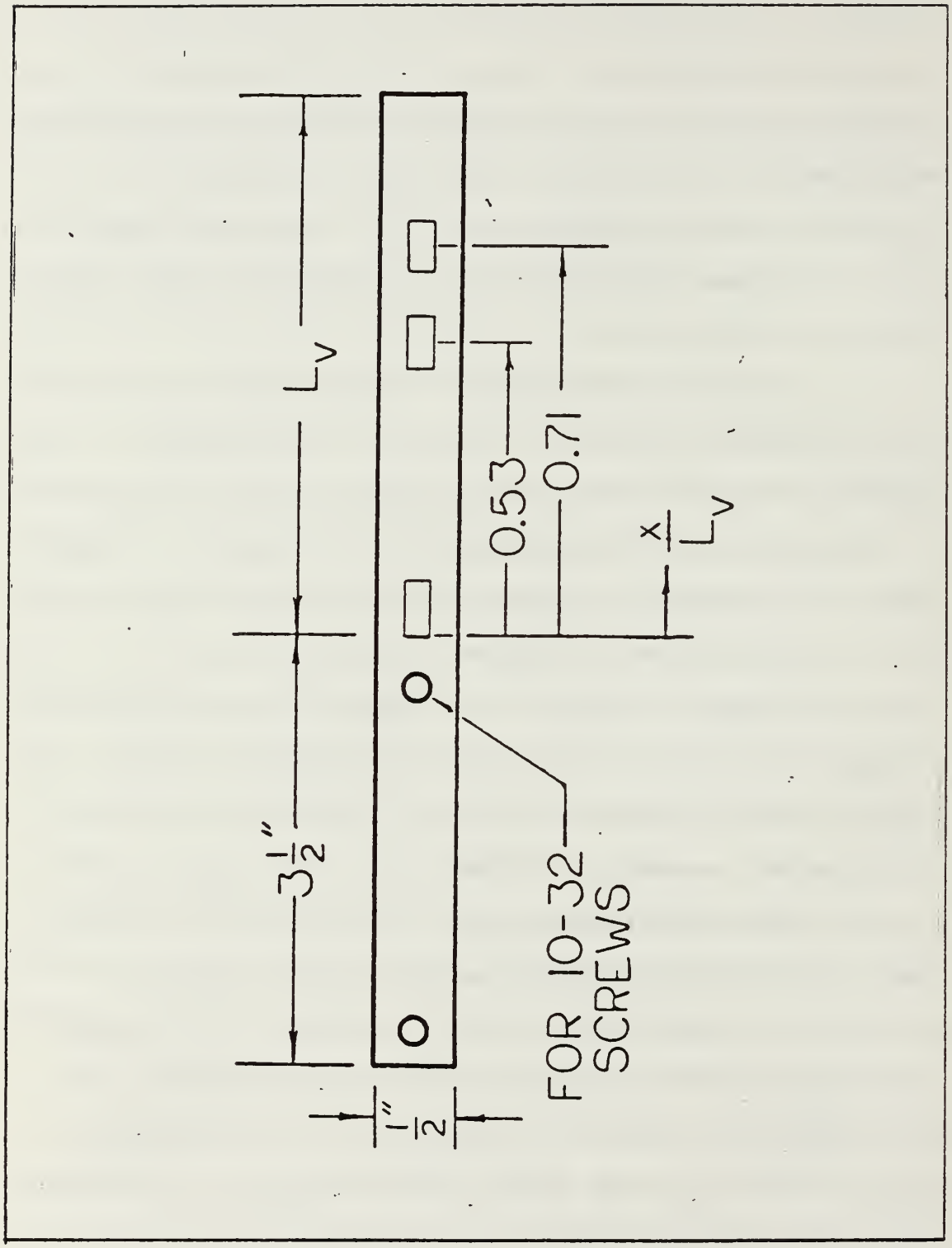

Figure 1.2 Specifications for Resonant Dwell Method Damping Specimens [Ref. 6:p. 44]

E. MICROSTRUCTURAL DAMPING MECHANISMS OF FERROMAGNETIC ALLOYS

As outlined previously, the microstructural mechanisms which contribute to high damping are:

- dislocation damping
- interphase boundary damping
- phase change effects

In ferromagnetic materials, damping generally is a function of two damping mechanisms. The damping caused by the magneto-mechanical hysteresis effect is the primary mode of damping. This damping mechanism is described by de Batist [Ref. 3:p. 43] under the catagory interphase boundary damping. A secondary mode of damping is due to the interaction of dislocations within the material [Ref. 25].

When a crystalline material is cyclically stressed, a number of microstructural mechanisms of damping may be activated. In ferromagnetic materials, this results in the magneto-mechanical effect. Ferromagnetic materials consist of domains, which are more or less randomly oriented in an unmagnetized material. Upon the application of a magnetic field, or a stress, these domains tend to align themselves in the direction of the tensile strain. The subsequent movement of these domains results in an irreversible change of the dimensions of the material called "magnetostriction". When a stress-strain curve for an unmagnetized ferromagnetic material is plotted, more strain is measured than postulated by Hooke's Law, and as stress is applied,

the domains tend to align themselves in a given direction. On relieving the load, the elastic strain reverts to zero (assuming negligible plastic deformation), but the magnetostrictive strain remains almost constant, i.e., the unloading curve follows a hysteresis loop. As described by Kuwabe and Kuwahara [Ref. 19:p. 32-33] for the response of SILENTALLOY (SIA) (Fe-Cr-Al alloy), in the absence of a magnetic field, the amplitude response indicates a shift of the resonance frequency to a lower frequency with increasing vibration force. The shift may be ascribed to the ΔE effect, i.e., the change in E (Young's Modulus) with magnetization; E depends on strain amplitude and on magnetization intensity, due to magnetostriction. The greater the area of the hysteresis loop, the larger the damping capacity of the material, from which it may be inferred that the damping capacities of high-strength ferromagnetic alloys are functions of magnetostriction and stress.

As described above, on the microstructural scale, the damping properties of the material are related to the movement of domain boundaries upon the application of stress. In their work with grain-oriented 3% Si-Fe, Schilling and Houze [Ref. 8] outlined the theory regarding the origin and actions of magnetic domains as follows:

1. Ferromagnetic domains are ferromagnetically ordered regions within which magnetization is equal to the saturation magnetism. Therefore, the net magnetization is a vector sum of the magnetization in all of the domains.

2. Upon the application of a magnetic field or external stress to a magnetic material, changes in the domain structure occur which produce changes in the overall specimen magnetization, as well as the specimen dimensions, i.e., "magnetostriction".

3. Response to changes in external field may be accomplished in either of two principle ways. Either magnetization within each domain may coherently rotate to a direction parallel to the applied field, or the boundary between two domains may move; in the latter case, the change in magnetization is entirely localized at the domain boundary.

In a material such as 3% Si-Fe, magnetocrystalline anisotropy is large, therefore domain rearrangements occur by the movement of domain boundaries or walls between domains. These walls are called Bloch walls [Ref. 26:p. 613] and are typically considered to be around 1000Å (angstroms) thick. Bloch walls serve in a manner similar to grain boundaries and are narrow zones in which the magnetic moment vector gradually and continuously changes from one domain to the next.

Another point of importance is the magnetic transition (Curie) temperature of the material. When the temperature of a ferromagnetic material is increased, the added thermal energy reduces the magnetic permeability (magnetization) and permits domains to become randomly oriented. Heating above the Curie temperature results in a complete transformation to a non-magnetic (paramagnetic) state in which the domains are randomly oriented throughout the material.

To summarize, the application of stress to a ferromagnetic material acts to align the domain structure in the direction of the stress. Under a weak magnetic field (or stress), the domains aligned with the applied field tend to grow at the expense of neighboring domains whose directions are less favorably oriented. As the field (stress) becomes stronger, it can also produce a rotation of the magnetic moment vector within domains toward the direction of the applied field (stress). [Ref. 22:p. 133] This domain movement results in an irreversible change in the dimensions of the material called magnetostriction. When the energy imparted to the system in the form of vibrations is utilized to produce this transformation, the resulting attenuation of the applied vibrational force constitutes damping, and turns out to be a relatively potent damping mechanism.

The relationship between the previously defined parameters of macrostructural damping and damping in ferromagnetic materials is provided by Cochardt [Ref. 7:p. 197-199] for damping capacity, magnetostriction, critical stress, and maximum stress. The damping capacity is expressed as the logarithmic decrement (δ)

$$\delta = (1/2)(\Delta U/U) \qquad \text{(eqn 1.10)}$$

where U = mean elastic energy of the specimen. This is directly related to our original definition of the logarithmic decrement by Thomson [Ref. 21:p. 34]

$$U = (1/V)(1/2)\int(\sigma^2/E)dV \qquad \text{(eqn 1.11)}$$

where ΔU is the energy dissipated in the entire specimen per cycle per unit volume [Ref. 7:p. 197]

$$\Delta U = (1/V)\int dU dV \qquad \text{(eqn 1.12)}$$

where dU is the energy loss per cycle and unit volume at the volume element dV. dU represents the area of the hysteresis loop described by the magneto-mechanical hysteresis. For small stresses, the area of the hysteresis loop is described by:[Ref. 7:p. 198]

$$dU = D\sigma^2 \qquad \text{(eqn 1.13)}$$

where D is a constant according to Rayleigh's law. For stresses larger than the maximum stress, beyond which the area of the hysteresis curve remains constant, the critical stress (σ_c): [Ref. 7:p. 198]

$$dU = K\lambda\sigma_c \qquad \text{(eqn 1.14)}$$

K = 4 for an ideal parallelogram-shaped loop

K = 1 for most other cases

λ = saturation magnetostriction in the easy direction of magnetization.

The assumption is made that Rayleigh's Law is valid up to the critical stress. Therefore, [Ref. 7:p. 198]

$dU = D\sigma^2$ $\qquad 0<\sigma<\sigma_c$

$dU = K\lambda\sigma_c$ $\qquad \sigma_c<\sigma<\sigma_m$

$D = K\lambda/\sigma_c^2$ $\qquad \sigma_m$ is maximum normal stress in a cantilever beam

Substituting the above relation into equation 1.12 and replacing dV by $(dV/d\sigma)d\sigma$ the logarithmic decrement becomes: [Ref. 7:p. 198]

$$\delta = (1/V)(K\lambda/2U)\left[\int_0^{\sigma_c}(\sigma^2/\sigma_c^2)(dV/d\sigma)d\sigma + \int_{\sigma_c}^{\sigma_m}\sigma_c(dV/d\sigma)d\sigma\right]. \qquad \text{(eqn 1.15}$$

As previously defined

$$Q^{-1} = \delta/\pi$$

Therefore,

$$Q^{-1} = (1/\pi V)(K\lambda/2U)\left[\int_0^{\sigma_c}(\sigma^2/\sigma_c^2)(dV/d\sigma)d\sigma + \int_{\sigma_c}^{\sigma_m}\sigma_c(dV/d\sigma)d\sigma\right] \qquad \text{(eqn 1.16)}$$

It should be noted that $dV/d\sigma$ is the stress distribution function. This can be evaluated in terms of the stress conditions of a cantilever beam:

$$\sigma = Mz/I \qquad \text{(eqn 1.17)}$$

where

M bending moment

z distance from the neutral axis of cantilever beam

I moment of inertia of rectangular cross section

For a cantilever beam, Cochardt defines the logarithmic decrement as: [Ref. 7:p. 199]

$$\delta = 9K\lambda E(\sigma_c/\sigma_m^2)(1-\sigma_c/\sigma_m((3/4)\ln(\sigma_m/\sigma_c)+ (15/16))) \qquad \text{(eqn 1.18)}$$

for $\sigma_c < \sigma_m$

As mentioned previously, damping capacity in a ferromagnetic material is a function of the magneto-mechanical hysteresis effect and to a lesser extent, dislocation damping.

As crystalline materials are cyclically stressed, they exhibit effects due to dislocation damping such that when a force is applied to it, dislocations move and energy is lost. Of course, if the applied force is high enough, the material will react plastically, which is characterized by an irreversible shape change.

With the increase in damping exhibited by a ferromagnetic material comes a maximum value of damping at a point of critical stress. Beyond this point, gradually decreasing values of damping are reported with increasing stress. This is attributable to a saturation condition for damping; the domains cannot grow or move any further. In addition to this, Degauque, Astie and Kubin [Ref. 25] report (in their experiments with high purity iron) that an interaction between 90° magnetic domain walls and dislocation tangles was evidenced. They found that dislocation tangles appear to be major obstacles to the motion of the magnetic domain walls. Single defects like isolated dislocations can interfere with small displacements of magnetic walls but, they cannot substantially oppose the large scale movement of these walls in the vicinity of the

maximum damping. Therefore an increase in dislocation density produces a decrease of the intensity of maximum damping and shifts it to higher shear strains.

F. METALLURGY OF THE IRON-CHROMIUM ALLOY SYSTEM

1. Physical Properties of Fe-Cr Alloys

The range of Fe-Cr binary alloys which are of interest as high damping ferromagnetic alloys are closely related to ferritic stainless steels, one of the three main classes of stainless steels (the other two being austenitic and martensitic alloys). Ferritic stainless steels are iron based alloys containing a nominal content of chromium ranging between 12 and 30 weight per cent. In general, ferritic stainless steels have seen much more restricted applications than austenitic stainless steels. The reason for this has been due to their susceptibility to embrittlement, notch sensitivity, and poor weldability; factors which contribute to poor fabricability. However, advantages in the use of ferritic stainless steels include high resistance to stress-corrosion cracking, and excellent corrosion and oxidation resistance. Ferritic stainless steels have also been considered in view of their excellent damping properties. For example, evaluation of the damping capacity of turbine blade alloys for the Wairakei, New Zealand geothermal power station and other future power stations was reported in 1982 [Ref. 27]. The

magneto-mechanical damping properties of an AISI 403 stainless steel were also investigated previously [Ref. 9].

Ferritic stainless steels are structurally quite simple. At room temperature, the Fe-Cr (α) solid solution has a body-centered crystal (bcc) structure. These alloys contain very little dissolved carbon, the majority of which appears in the form of more or less finely divided chromium carbide precipitates.

Examination of the Fe-Cr binary phase diagram (Figure 1.3) reveals a great deal of activity in the range 11% to 12% Cr content region. As outlined by Peckner and Bernstein [Ref. 28:pp. 5-2 - 5-3] the following relationships and potential transformations exist:

- As a member of a group of elements described as ferritic stabilizers, chromium extends the (α) phase field while narrowing and suppressing the gamma (γ) face-centered (fcc) phase field. As evidenced in Figure 1.3, this creates a "gamma loop" extending in temperature range from 850°C to 1400°C.

- Whereas the transformation from α to γ phase occurs in pure iron at about 910°C, as chromium is added a depression of the transition temperature occurs to about 850°C at 8% chromium, then rapidly increases to about 1000°C as the chromium content reaches 12% to 13%.

- Whereas in pure iron the transformation from γ to α occurs at about 1400°C, this reaction is depressed to about 1000°C in the 12% to 13% Cr range. Also occuring at this point in the phase diagram (1000°C, 12% to 13% Cr) is a joining of the upper and lower temperature α:γ curves to close off and form the gamma loop. Beyond 12% to 13% Cr,

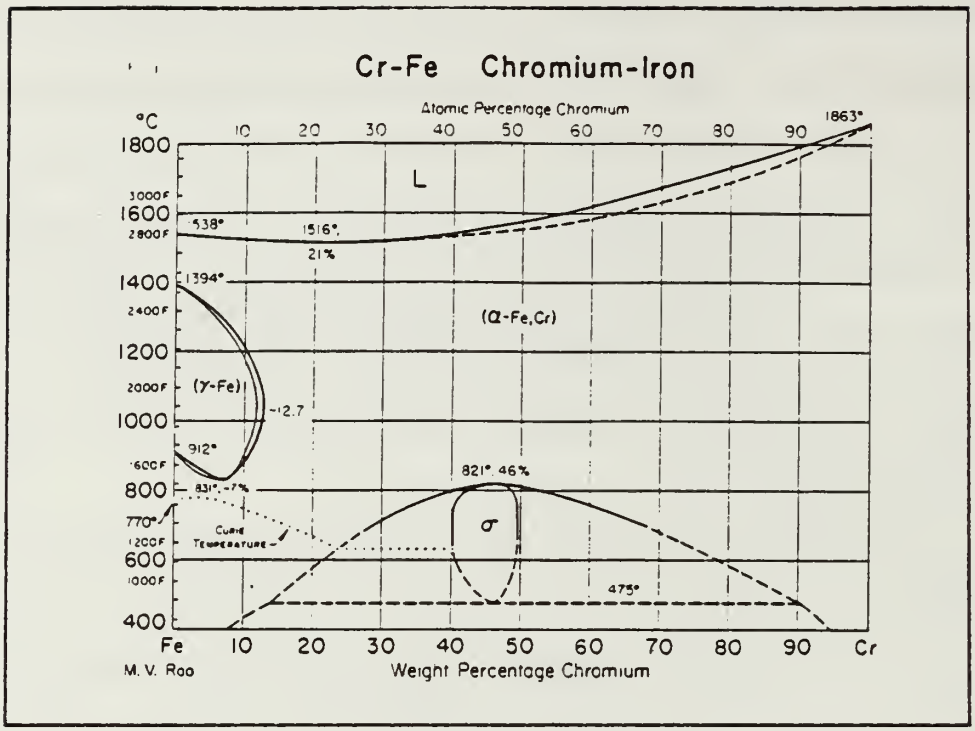

Figure 1.3 Fe-Cr binary phase diagram [Ref. 29]

transformation to γ is no longer possible and an alloy would remain ferritic (bcc) over the entire range from room temperature to melting.

- Between the extensive α phase field and the γ loop, there is a relatively narrow transition region where the alloy can have both α and γ phases. Because of the limited extent of this two phase region, depending on the annealing temperature, alloy composition and quench rate, this two phase region may or may not be retained upon cooling to room temperature.

The physical parameters of the γ loop have been established for the Fe-Cr binary system through the work of Baerlecken, Fisher, and Lorentz [Ref. 28:p. 5-3]. Using magnetic measurements at elevated temperatures, the lowest point in the γ loop was identified at 840°C and 6.5% Cr. The greatest width of the α and γ phase field occured at

1075°C and reached to about 11.5% Cr. Variations in the extent of the γ loop were found to be very much a function of the addition of austenizing elements, particularly carbon and nitrogen. Increasing levels of these interstitial elements causes the γ loop to extend to higher chromium levels (see Figure 1.4).

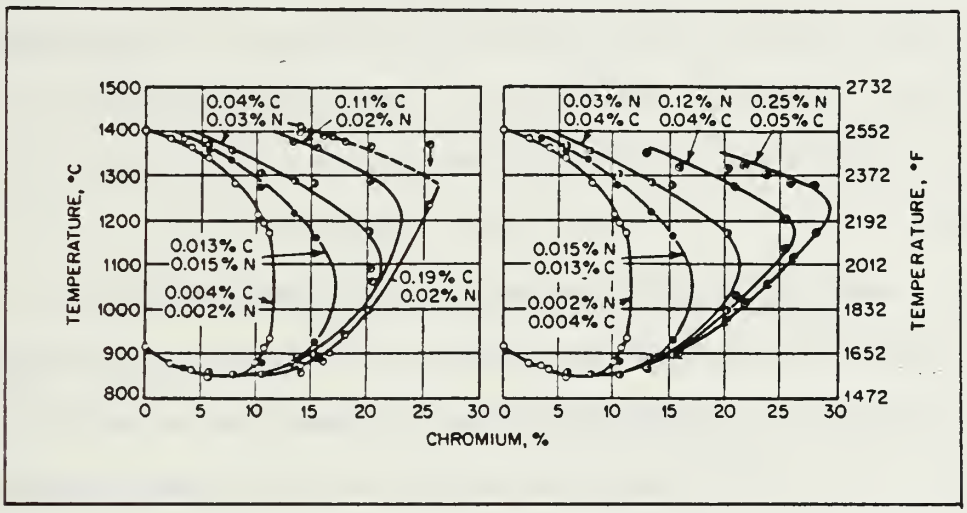

Figure 1.4 Shifting of the boundary line (γ+α)/α in the Fe-Cr system through the addition of carbon and nitrogen [Ref. 28:p. 5-4]

Another effect of carbon is that because of its low solubility in the α phase, excess carbon is rejected from solid solution to form complex carbides, such as $(Cr,Fe)_7C_3$ and $(Cr,Fe)_{23}C_6$, which precipitate predominately along grain boundaries.

The strengthening mechanisms normally characteristic of stainless steels do not extend to the ferritic stainless steels. Ferritic stainless steels are

characterized by the absence of an $\alpha \rightarrow \gamma$ transition upon heating to high temperatures. Consequently, the hardening of the material that occurs as a result of a $\gamma \rightarrow$ martensite transformation upon cooling will not normally occur.

The largest single drawback to the use of ferritic stainless steels has been a loss of corrosion resistance and ductility following exposure to high temperatures. However, the addition of molybdenum (Mo) improves the corrosion resistance of ferritic stainless steels.

2. Damping Properties of Fe-Cr Alloys

The damping properties of Fe-Cr alloys are attributable to the magneto-mechanical hysteresis mechanism associated with ferromagnetic materials. This mechanism is a function of the material in which it operates and is directly related to the physical state of the material and the associated microstructure. The following physical parameters affect the domain wall mobility of the material and subsequently the damping capacity.

a. Strain or Stress [Refs. 7,9-11,13-15,16,17,19]

In general, damping capacity increases with applied stress or strain. However, the degree to which stress influences damping depends on the alloy's thermo-mechanical history. Additionally, it has been reported

many times that damping will reach a maximum value with stress beyond which further stressing will lower damping values.

b. Cold Work [Refs. 14,15,24]

The damping capacity is strongly deteriorated by cold work. A reduction of ≥ 5% completely destroys the damping effect; however, it can be fully restored by a succeeding heat treatment.

c. Magnetic Field [Refs. 7,9,12-15,18,30]

At high fields, the domain walls become fixed; i.e., the damping capacity decreases and finally disappears. Therefore, these alloys should not be used in applications where there are stray magnetic intensity fields greater than the range of 50-100 A/cm.

d. Magnetic (Curie) Transformation Point [Refs. 26,28]

The magnetic transformation temperature, otherwise known as the Curie temperature, is the point above which iron is paramagnetic and, below which is ferromagnetic. Paramagnetic iron is nonmagnetic (permeability = 1.00). Ferromagnetic iron is magnetic (permeability > 1.00, the magnitude varying with composition). If fcc (γ) austenite is maintained to lower temperatures the alloy will remain paramagnetic. At room temperature γ-austenite is nonmagnetic while α-ferrite (bcc) is ferromagnetic. Therefore, the magnetic

composition and hence the ultimate damping capacity is affected by the degree of paramagnetism evident in the structure.

II. EXPERIMENTAL PROCEDURES

The alloy VACROSIL-010 (Mo) was supplied by David W. Taylor Naval Ship R & D Center, Annapolis Laboratory, in the form of a circular plate (13.0 inch diameter X 0.5 inch thick). The actual composition of the alloy was determined by Anamet Laboratories, Inc., of Berkeley, California as:

	Fe	Cr	Mo	Cu	Mn	Si	remainder
w/o	84.66	11.28	2.45	0.97	0.34	0.21	0.09

All specimens were annealed for 1 hour in a tube furnace under flowing argon gas at temperatures of 800°C, 900°C, 1000°C, and 1100°C. A set of specimens from each temperature was furnaced cooled under flowing argon gas, while a second set was water quenched. All samples were stored at room temperature until required for testing.

Subsize tensile specimens were cut from the as received plate in accordance with Reference (31). Tensile tests for heat treated samples were conducted on an Instron Universal Testing Instrument Model TT-D at a strain rate of 3.33×10^{-3} sec^{-1}. Tensile tests to fracture, for specimens furnaced cooled and water quenched from each annealing temperature (800°C, 900°C, 1000°C, 1100°C) were conducted at ambient temperature. Subsequently, tensile load-unload tests at low strains were conducted on furnace cooled samples (900°C and 1100°C) in an effort to observe in more

detail the apparent region of stress-strain nonlinearity detected in the earlier tests and to determine if a pseudoelastic region existed. Rockwell B (R_B) hardness readings were taken after tensile testing, using a Wilson Rockwell Hardness Tester Model 1JR (B scale, 1/16 inch ball, 100 KILO Load). Fracture surfaces were examined using a Cambridge Scanning Electron Microscope.

Specimens for optical microscope examination were prepared from the tensile samples. Specimens mounted in bakelite were mechanically ground using silicon carbide (SiC) in a grit sequence of 240, 320, 400 and 600. 3/0 emery paper was then used prior to polishing. Hand polishing was done on 8 inch rotating wheels using short nap cloth. The polishing sequence prior to final polish was accomplished using diamond polishing compound (15 micron, 6 micron, 1 micron) followed by a final polish using 0.05 micron Aluminum Oxide Slurry (Al_2O_3). Samples were etched in Kallings No. 2 etch for 20 seconds, followed by ultrasonic cleaning between polishing stages. The final etch was for 30 seconds. Standard metallographic procedures were followed. [Ref. 29:pp. 1-8]

Lattice parameters were determined by X-ray diffraction for each heat treatment. A Phillips XRG-3100 X-ray diffractometer was used with a copper target tube at a scan rate of 1/2 degree per minute. The specimens analyzed were powder samples ground using a fine file.

The mass density (ρ) for each heat treatment was determined from the specimens used for X-ray diffraction analysis prior to filing.

Damping measurements were done at room temperature using a modified resonant dwell technique and the apparatus used in previous investigations of material damping at the Naval Postgraduate School (Figure 2.1) [Ref. 15:pp. 37-45]. Damping specimens were cut to the specifications [Ref. 23:p. 20] for the resonant dwell method. (See Fig. 1.2) The variable dimensions of thickness and vibrating length were selected as approximately 0.08 inches and 7.0 inches, respectively. These resulted in a nominal mode 1 resonance at 49.2Hz, with the resonant frequencies for mode 2 and 3 corresponding to 308.4 Hz and 863.43 Hz, respectively. Slight variations in specimen density and thickness of the beams resulted in a small frequency range variation of the modes between individual specimens. Some interference in frequency response curves was experienced during Mode 1 excitation. This was probably attributable to some degree of stray magnetic interference from the electromagnetic shaker, though this effect diminished with increasing applied load. The exact specimen dimensions are provided in Table 2.

TABLE 2

DAMPING SPECIMEN DIMENSIONS PRIOR TO TESTING

HEAT TREATMENT (1 hr anneal, °C)	THICKNESS (inch)	WIDTH (inch)	VIBRATING LENGTH (inch)
800 FURNACE COOL	.0763	.5262	7.00
800 WATER QUENCH	.0786	.5229	7.00
900 FURNACE COOL	.0773	.5250	7.00
900 WATER QUENCH	.0774	.5217	7.00
1000 FURNACE COOL	.0785	.5214	7.016
1000 WATER QUENCH	.0796	.5242	7.00
1100 FURNACE COOL	.0808	.5237	7.00
1100 WATER QUENCH	.0772	.5241	7.00

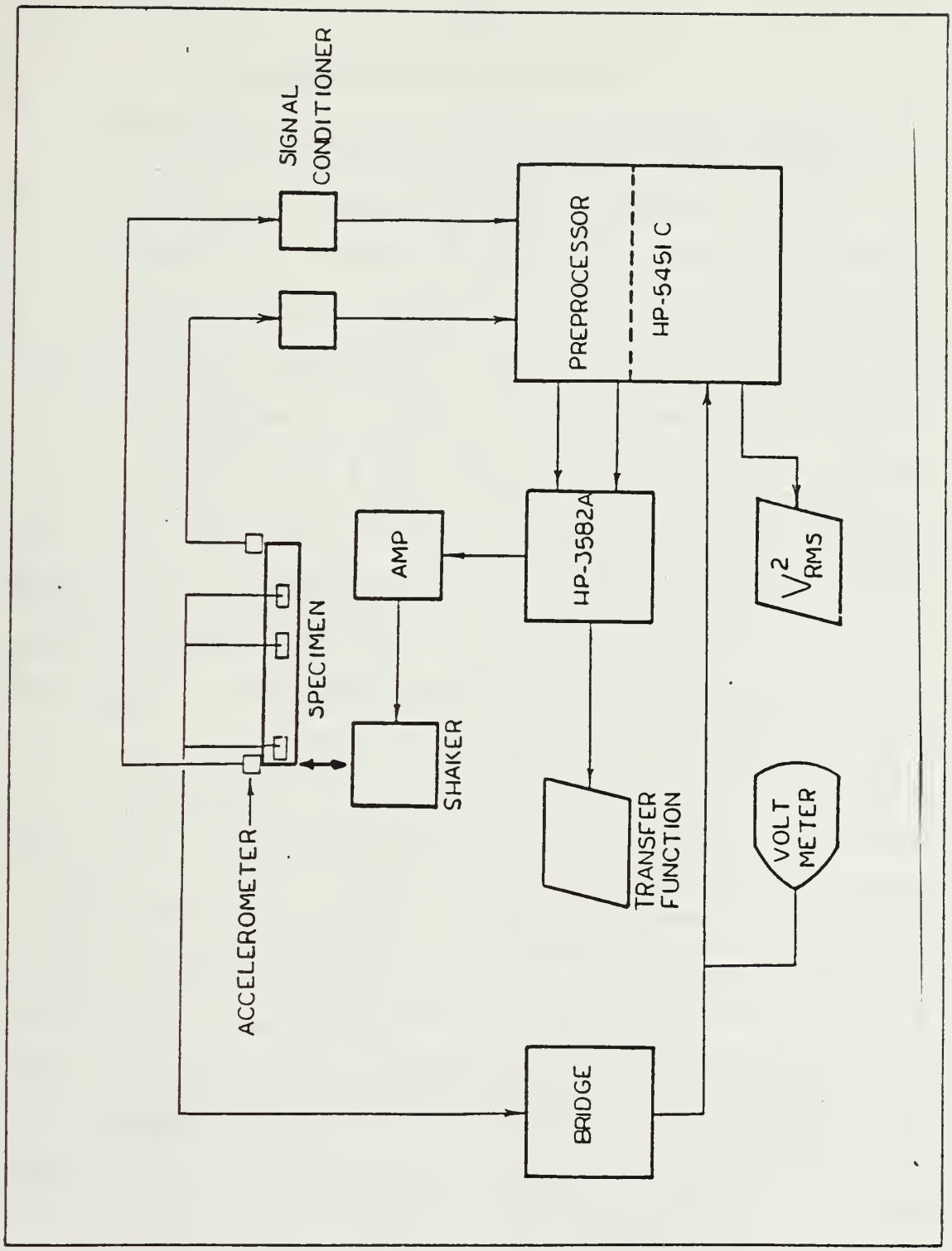

Figure 2.1 Block Diagram of Damping Experiment Components
[Ref. 6:p.40]

III. RESULTS AND DISCUSSION

A. DAMPING CHARACTERISTICS OF VACROSIL-010 (Mo)

The relationship of specific damping capacity (SDC) to average peak strain, ϵ_{peak}, for VACROSIL-010 (Mo), is presented in Figures 3.1 through 3.8. In Figures 3.1, 3.2, 3.3, and 3.4, the SDC values for specimens furnace cooled and water quenched from each annealing temperature are shown. It is evident that there is a significant difference in SDC between the two cooling conditions. The damping values for water quenched samples are, for the most part, relatively consistent (ranging between approximately 5% to 15%) with very little strain dependence. The furnace cooled specimens, on the other hand, demonstrate significantly higher values of SDC and a strong strain dependence. Figures 3.5 through 3.8 reflect the SDC values at each mode of damping for the furnace cooled specimens from each annealing temperature. This data demonstrates that with increasing cyclic strain amplitude, the furnace cooled specimens exhibit increasing SDC to a maximum, then display a slightly decreasing trend with increasing strain. The values of peak damping and peak strain (ϵ_{peak}) at peak damping are tabulated for each furnace cooled condition in Table 3.

TABLE 3

MAXIMUM SDC VS. PEAK STRAIN

ANNEALING TEMP	SDC (%)	ϵ_{peak} (x 10^{-5})
800°C	36.214	15.596
900°C	49.005	6.714
1000°C	36.349	12.639
1100°C	54.717	7.172

As mentioned in section I. E., the microstructural damping mechanism in an Fe-Cr alloy is predominately the result of the magneto-mechanical hysteresis effect. As demonstrated by the furnace cooled SDC data, upon the application of cyclic loading to this material, significant damping becomes evident at quite low strains, with a very sharp increase in SDC with increased strain. This corresponds to the attenuation of vibrational energy as this energy is used to align domains in the direction of loading and results in magnetostriction. One of the supposed purposes of annealing these alloys at high temperatures is to relieve residual stresses. This is because whereas the application of stress to the material activates the magneto-mechanical hysteresis effect, the existance of prestress (residual stress) acts in the same way as a weak magnetic field applied to the material, and domains whose directions are favorably aligned with respect to the stress tend to grow at the expense of the neighboring domains whose directions are less favorably oriented. Thus, as a cyclic load is applied to a material,

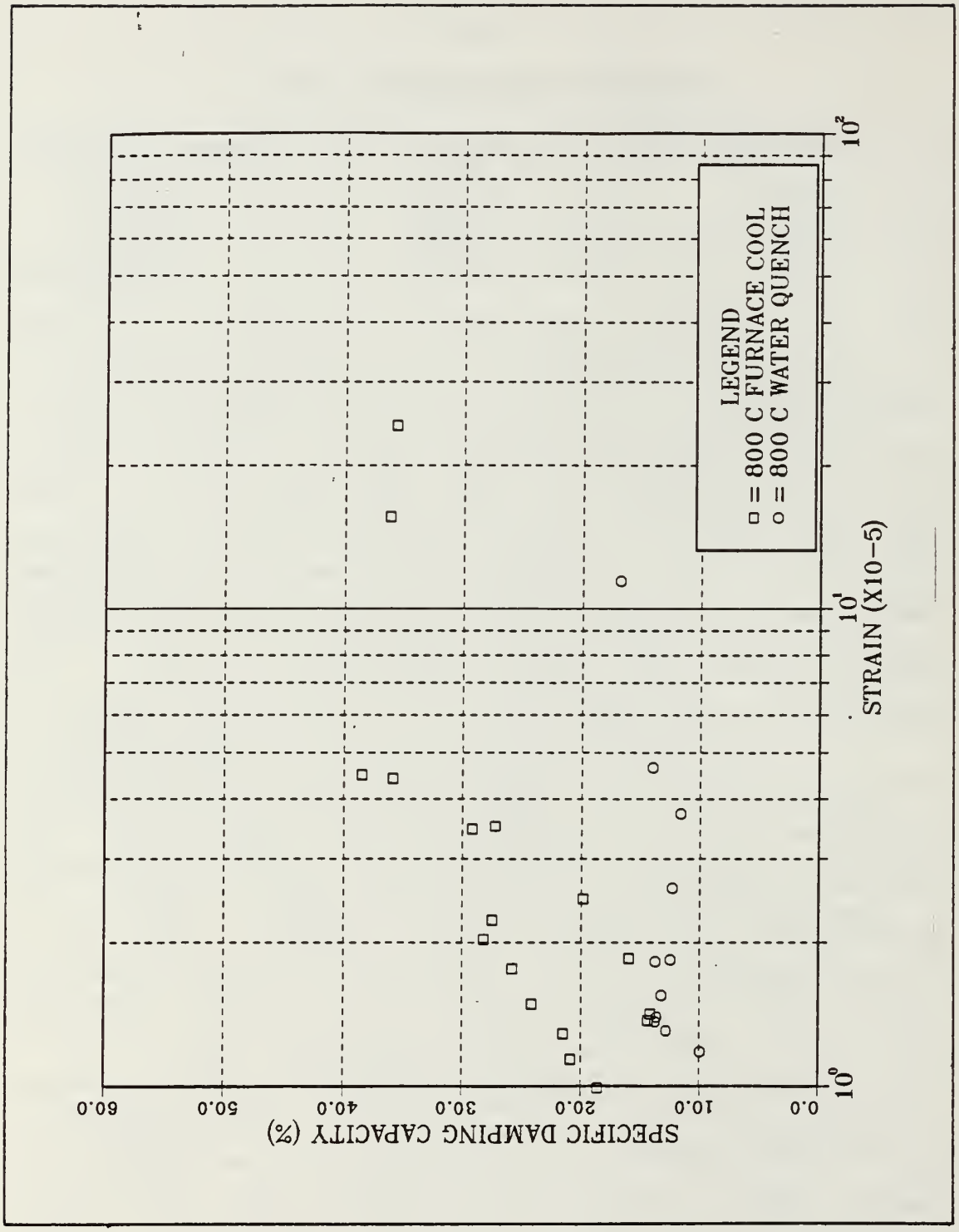

Figure 3.1 Damping Characteristics of VACROSIL-010(Mo) Annealed at 800°C (Furnace Cool and Water Quench Specimens)

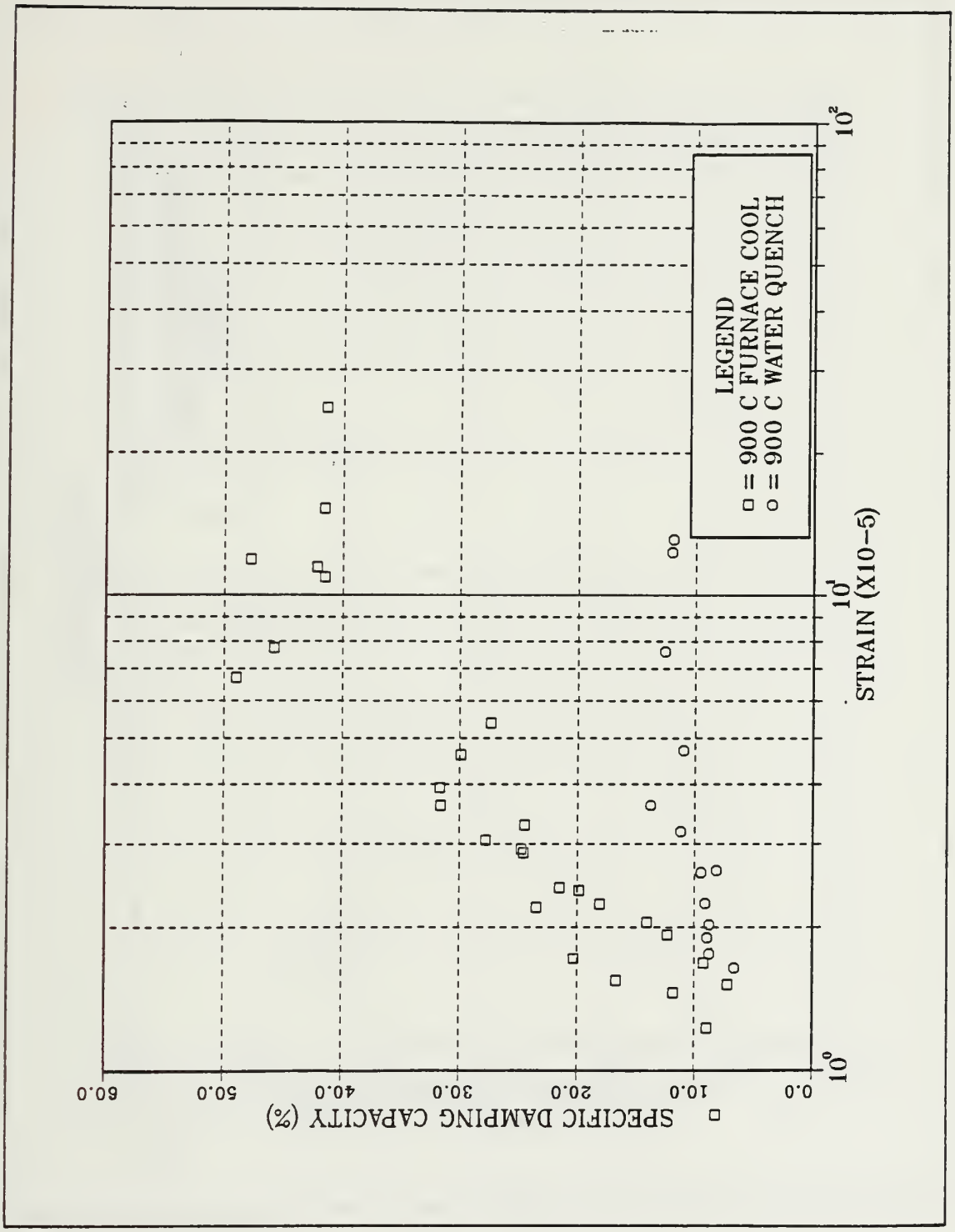

Figure 3.2 Damping Characteristics of VACROSIL-010(Mo) Annealed at 900°C (Furnace Cool and Water Quench Specimens)

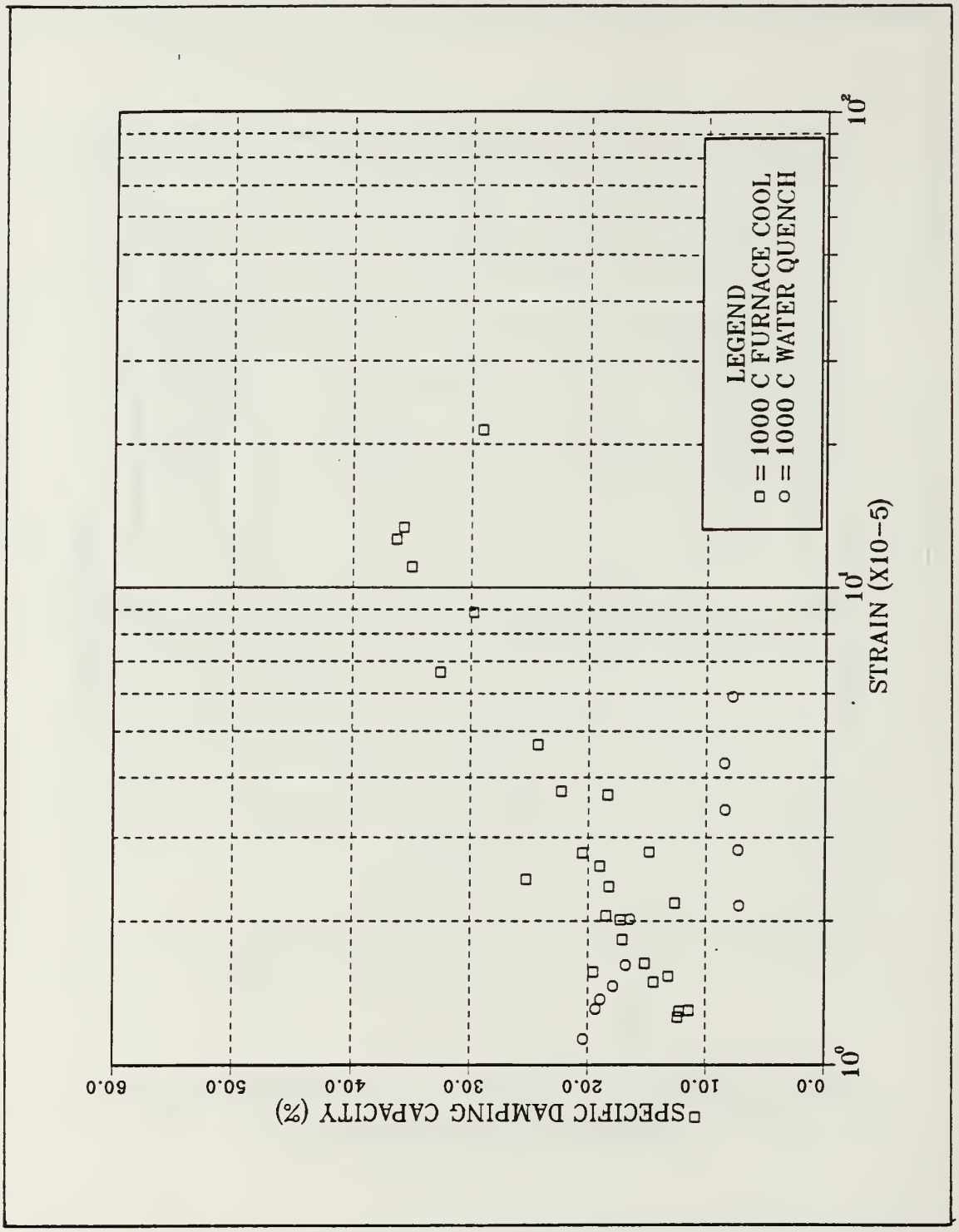

Figure 3.3 Damping Characteristics of VACROSIL-010(Mo) Annealed at 1000°C (Furnace Cool and Water Quench Specimens)

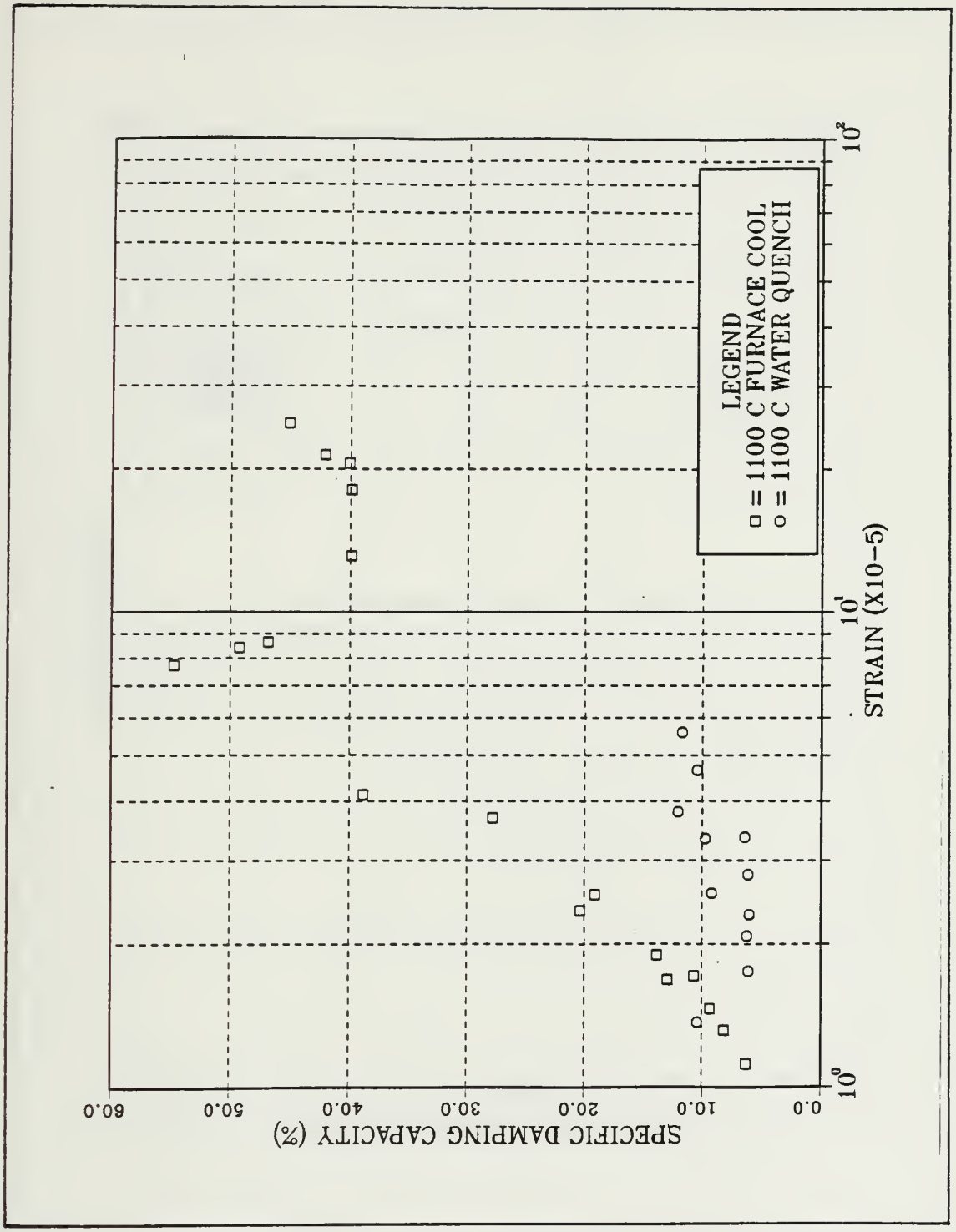

Figure 3.4 Damping Characteristics of VACROSIL-010(Mo) Annealed at 1100°C (Furnace Cool and Water Quench Specimens)

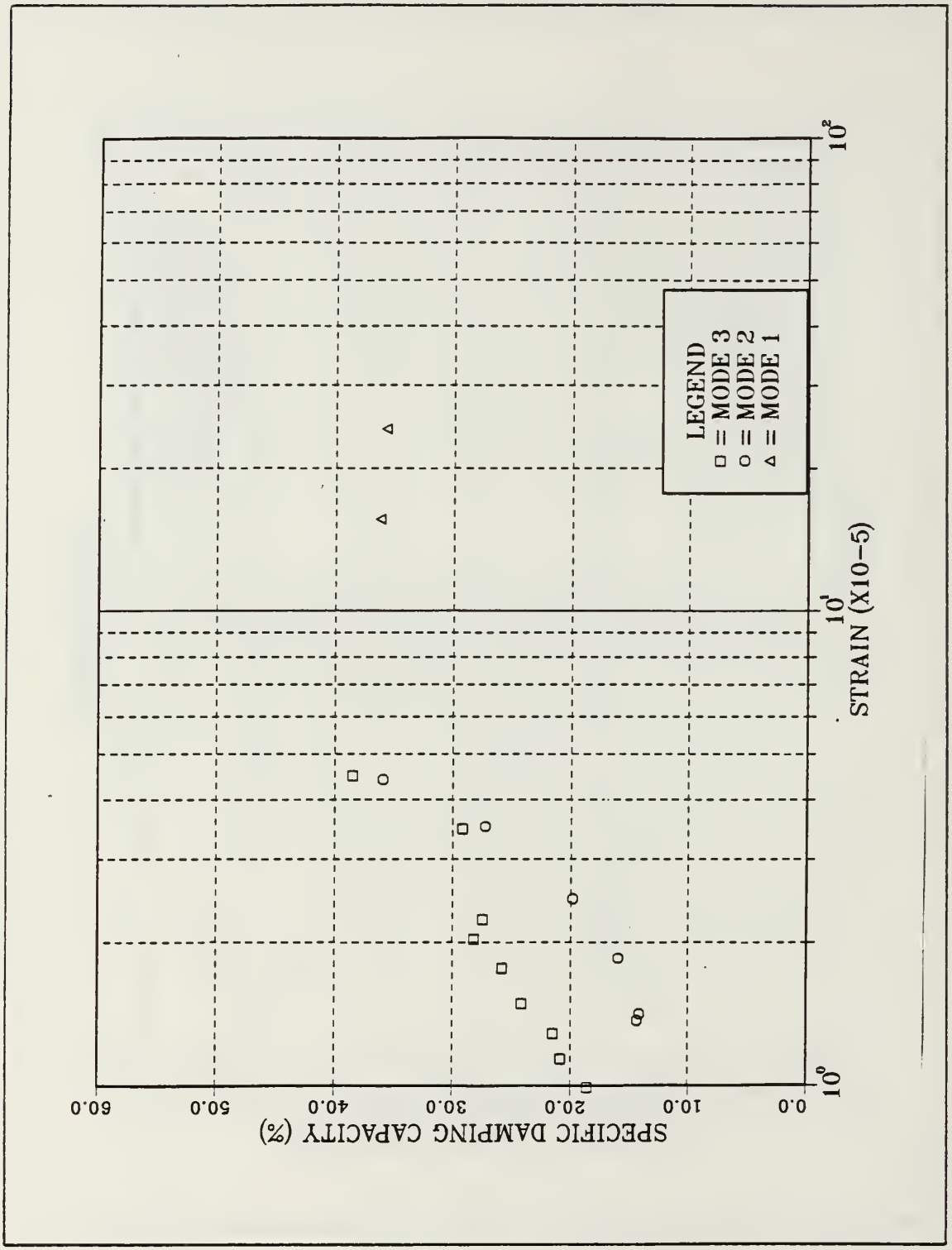

Figure 3.5 Mode 1,2 and 3 Damping Characteristics of VACROSIL-010(Mo) (800°C Furnace Cool)

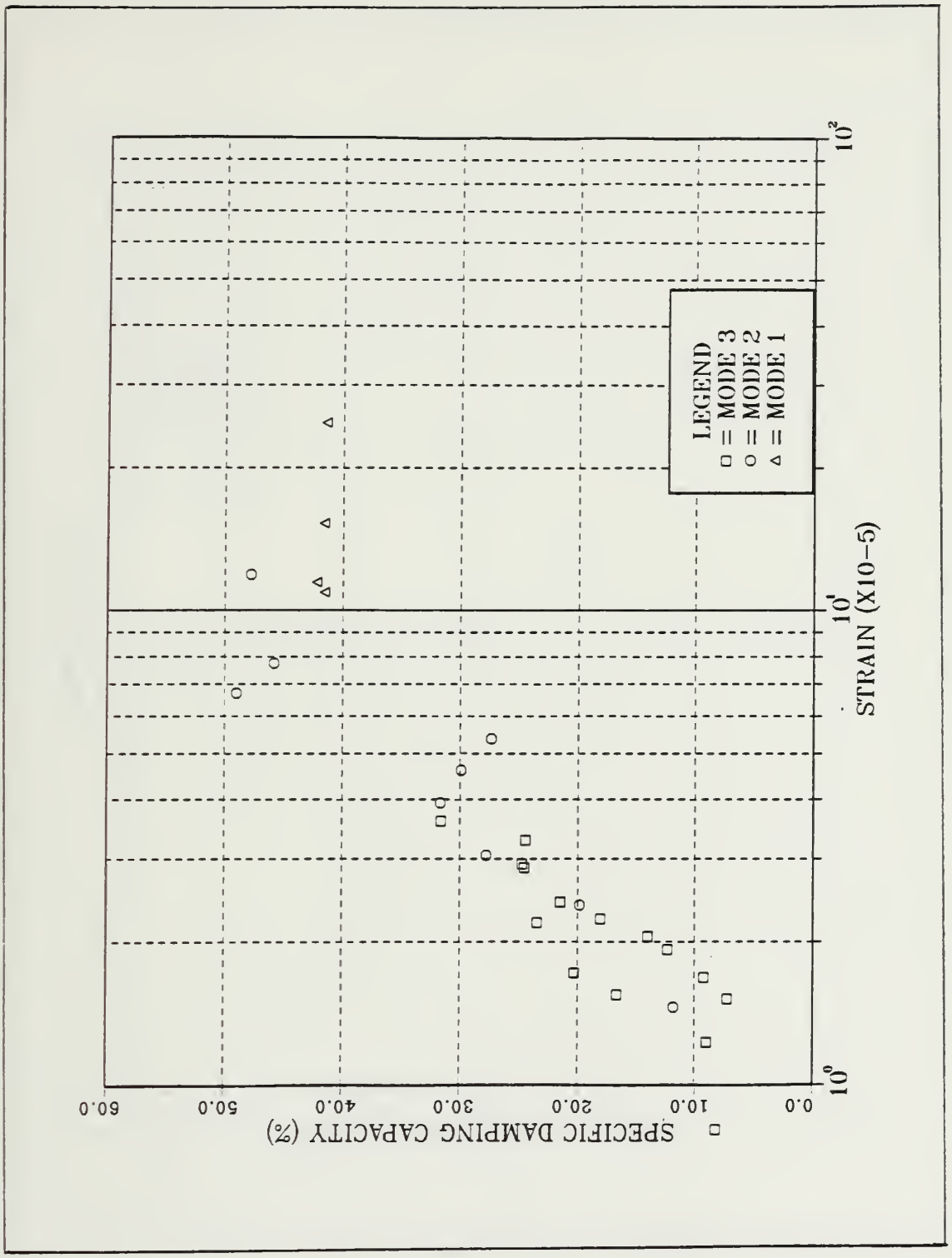

Figure 3.6 Mode 1,2 and 3 Damping Characteristics of VACROSIL-010(Mo) (900°C Furnace Cool)

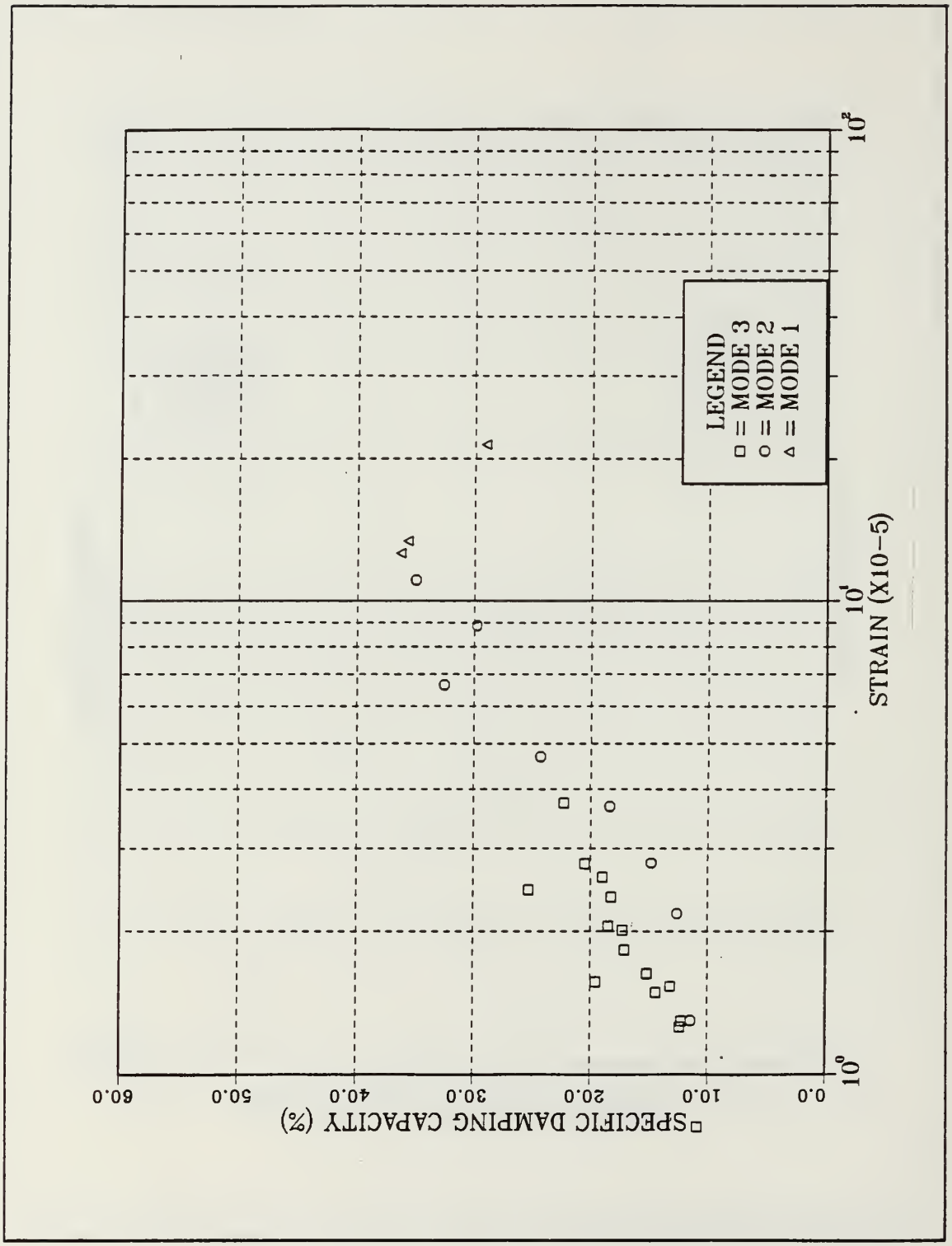

Figure 3.7 Mode 1,2 and 3 Damping Characteristics of VACROSIL-010(Mo) (1000°C Furnace Cool)

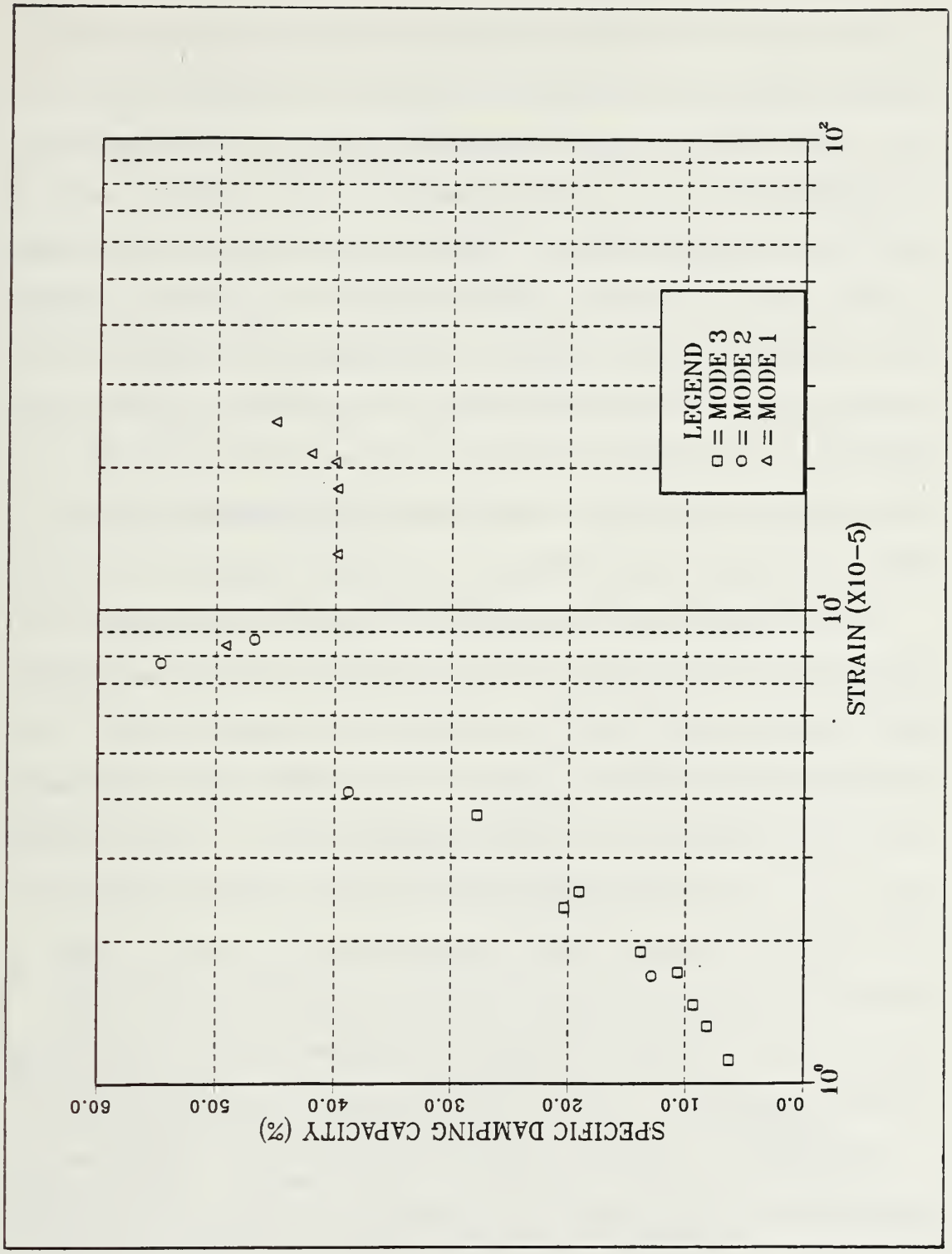

Figure 3.8 Mode 1,2 and 3 Damping Characteristics of VACROSIL-010(Mo) (1100°C Furnace Cool)

the extent to which the domains can rotate and that the Bloch walls can move has been limited by the pre-stress, thus resulting in lower levels of damping. In comparing the resultant damping capacities of furnace cooled and water quenched specimens, it may be speculated that furnace cooling allows the material to cool at a rate slow enough to minimize residual stress in the material. Water quenching the specimens obviously results in a higher residual stress level within the material, such as to substantially interfere with the damping mechanism and result in significantly lower levels of damping.

When considering the effect of initial annealing temperature on furnace cooled specimens, an increase in peak damping was noted as the annealing temperature increased, with the exception of the 1000°C heat treatment. The 1000°C temperature heat treatment gave a lower peak SDC than those recorded at 900°C and 1100°C (furnace cooled specimens). No deviations in experimental procedure were noted at this temperature. This may indicate that some other factor besides the residual stress state is having an effect on damping; further discussion of this will follow.

In previous damping studies on ferromagnetic alloys, a charateristic sharp peak of damping with strain, followed by a rapid decrease was typically observed. In most of these earlier studies, damping was evaluated using the inverted torsion pendulum method, with free decay

vibrational conditions. As noted by Cochardt [Ref. 7:p. 197], in a torsional oscillation system, the volume where the shear stress becomes a maximum divided by 2, or smaller, is 25%. In a cantilever beam, the volume where the stress is a maximum divided by 2, or smaller, is 85%. In other words, in the case of the cantilever beam, the unsaturated magneto-mechanical hysteresis mechanism operates in a large part of the beam. On the other hand, for a torsion pendulum, the saturated hysteresis operating volume is predominant. Therefore, at a higher stress (strain) than the critical one (peak), it is supposed that the possibility of added damping from the high stress damping mechanism is less in the torsional system than in the cantilever beam arrangement. This is confirmed by the present furnace cooled data, which indicates a much broader strain range for high damping than has been indicated by previous data from the torsional pendulum.

B. OPTICAL MICROSCOPIC EXAMINATION OF VACROSIL-010

An attempt was made to correlate the damping characteristics evident in VACROSIL-010 with the microstructure at the optical microscopic level of examination. As mentioned previously, the Fe-Cr-based alloys of interest as high damping ferromagnetic alloys are closely related to ferritic stainless steels. VACROSIL-010(Mo) with a measured chromium content of 11.28 weight %, falls into this category. It was noted in section I. F.

that on the equilibrium binary Fe-Cr phase diagram (Figure 1.3), a chromium content of 11.28% lies quite close to the two phase ($\alpha + \gamma$) region at annealing temperatures employed. It was also noted that the range of this two phase region, and its shape, are affected by carbon and nitrogen content (Figure 1.4), the initial parameters of the phase being established based on Fe-Cr alloys with a carbon content of 0.004% C and 0.002% N [Ref. 28:p. 5-3]. For the VACROSIL-010(Mo) used in this work, carbon and nitrogen contents of approximately 0.001% and 0.004%, respectively, were measured. Based on this information and examination of the binary Fe-Cr phase diagram, it is reasonable to assume that the extent of the ($\alpha + \gamma$) region being considered is very similar to that of the Fe-Cr binary diagram (Figure 1.3). At 800°C and 900°C, we are below the nose of the ($\alpha + \gamma$) phase region. At 1000°C, it would appear that the composition of VACROSIL-010(Mo) places it just within this region; while at 1100°C we are quite close to the edge of the ($\alpha + \gamma$) phase but probably just above it. Examination of the ternary phase diagrams for Fe-Cr-Mo at isothermal sections of 900°C and 1250°C (Figure 3.9) demonstrates the possibility of the formation of several intermetallic phases, most notably a χ (chi) phase described as a cubic structure of approximate composition $Fe_{36}Cr_{12}Mo_{10}$ or Fe_3CrMo. [Ref. 29:p. 421]

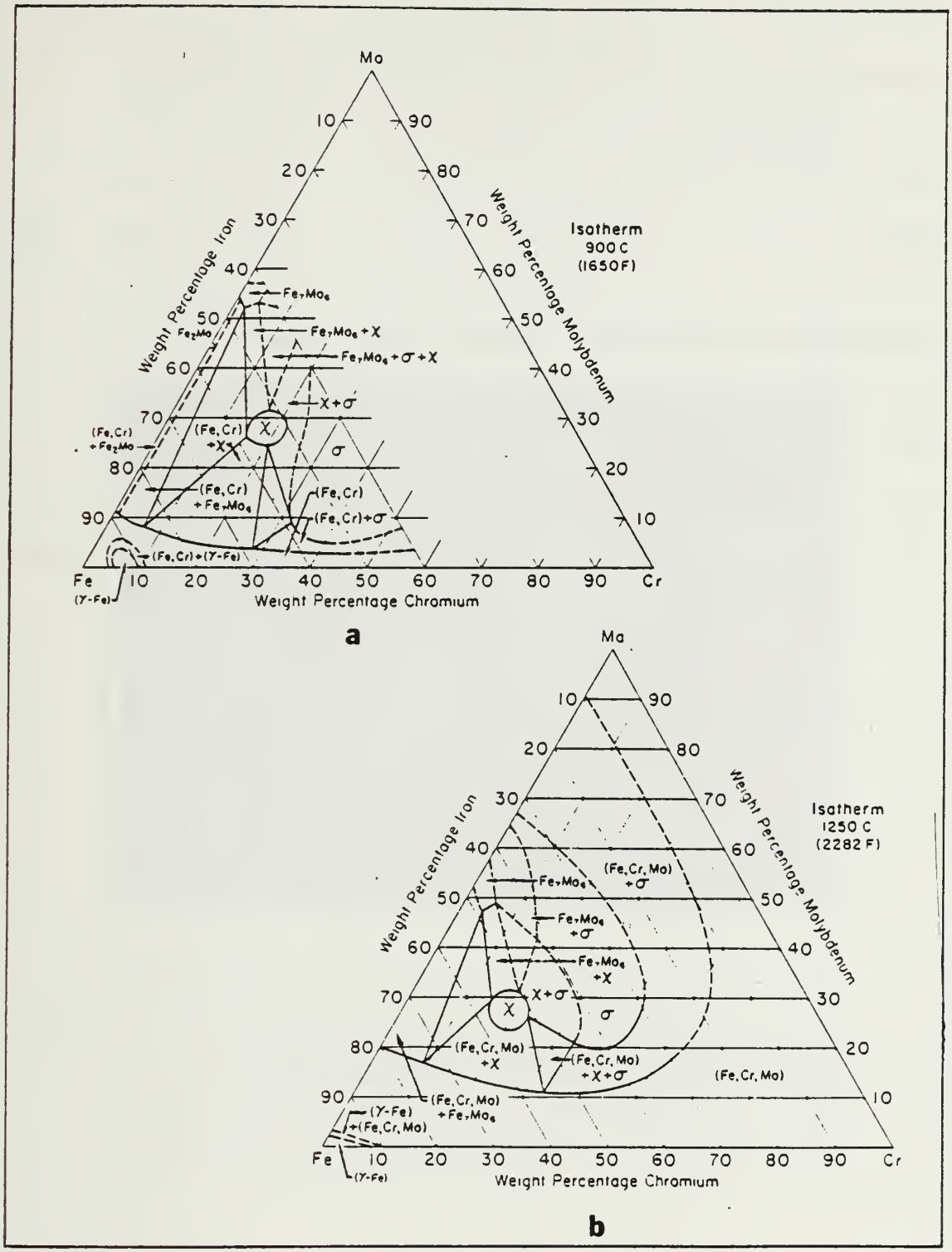

Figure 3.9 Ternary Phase Diagrams for Fe-Cr-Mo at (a) 900°C and (b) 1250°C Isotherm [Ref. 29]

Actual examination of the microstructure via optical microscopy produced no direct correlation between it and the damping capacity of the material. The microstructure was characterized by quite large grains, to be expected from grain growth at the high annealing temperatures. The formation of a second phase, located at the grain boundaries, was evident only for the furnace cooled specimens; this is possibly the intermetallic χ phase. This was not evident for the water quenched specimens. Also, a subgrain structure was noted for samples cooled from 1100°C (Figure 3.10). Examples of the microstructure are depicted by Figures 3.11 through 3.18.

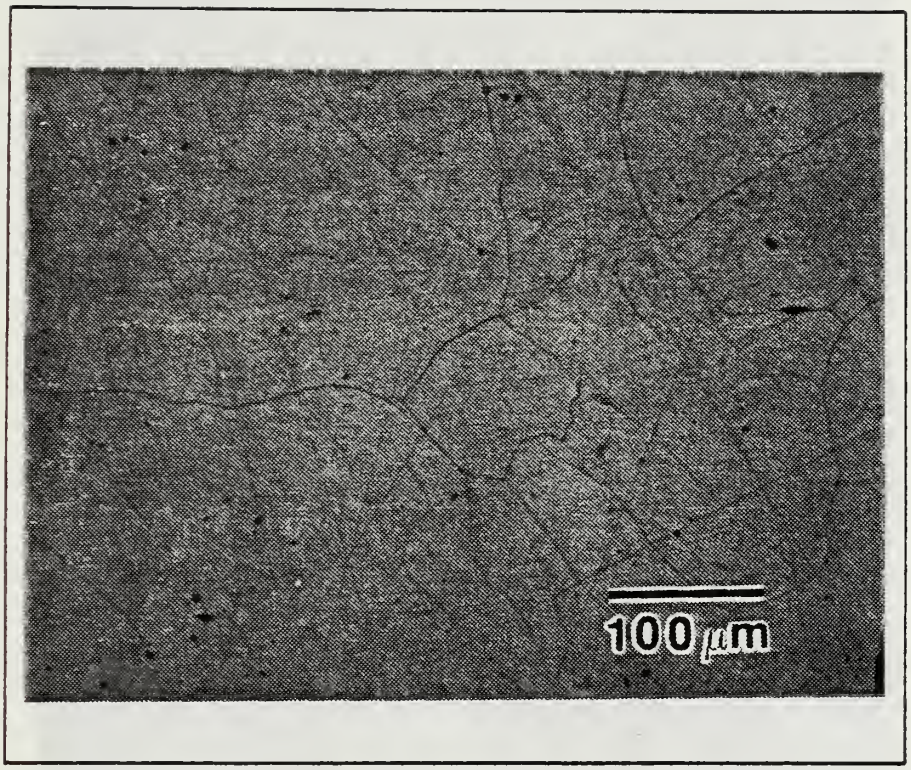

Figure 3.10 Optical Micrograph of Furnace Cooled VACROSIL-010(Mo) Annealed 1 Hour at 1100°C (200X). Subgrain Structure Evident Within the Large Grains.

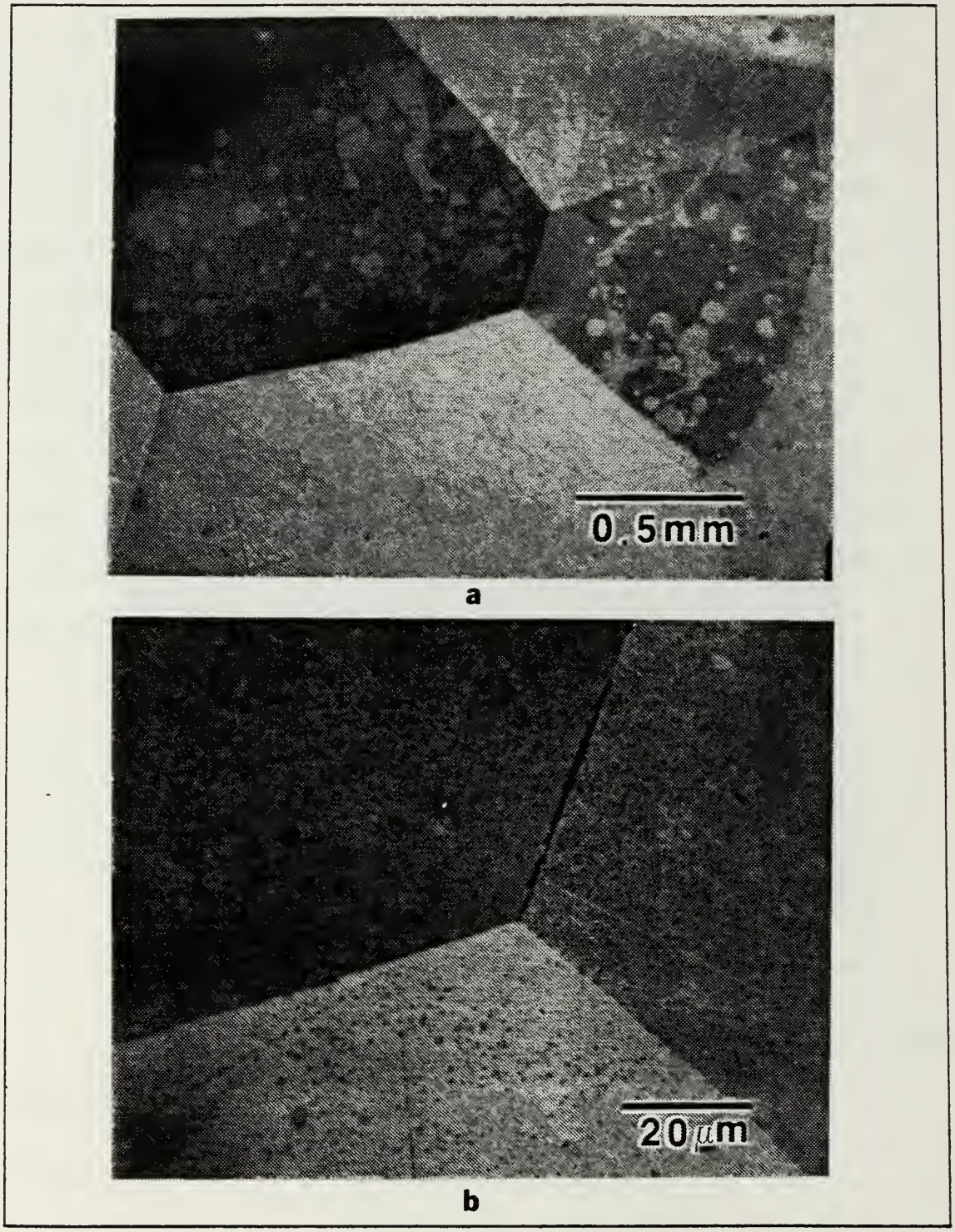

Figure 3.11 Optical Micrograph of Furnace Cooled VACROSIL-010(Mo) at (a) 50X and (b) 1000X Annealed 1 Hour at 800°C.

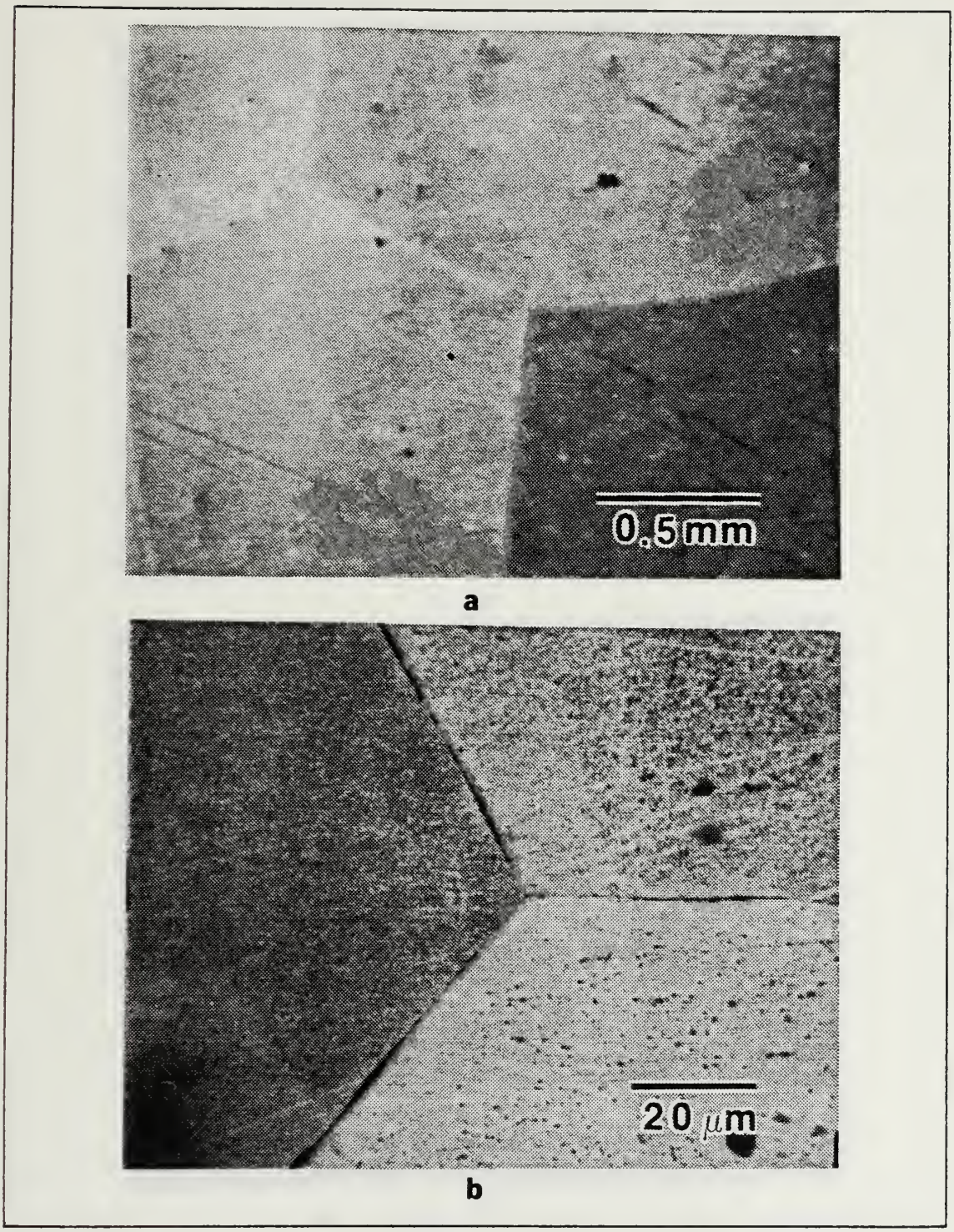

Figure 3.12 Optical Micrograph of Furnace Cooled VACROSIL-010(Mo) at (a) 50X and (b) 1000X Annealed 1 Hour at 900°C.

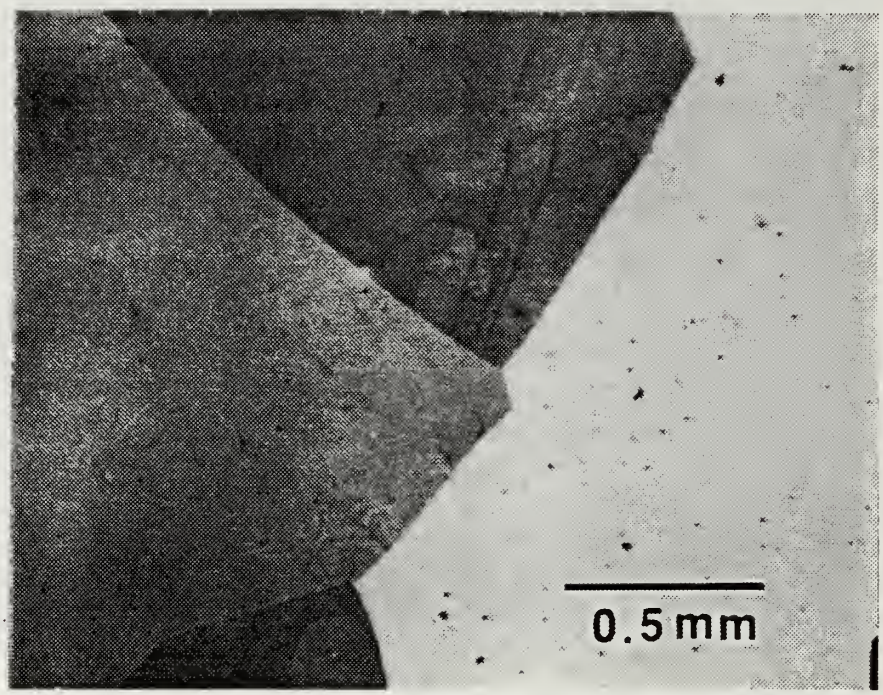

a

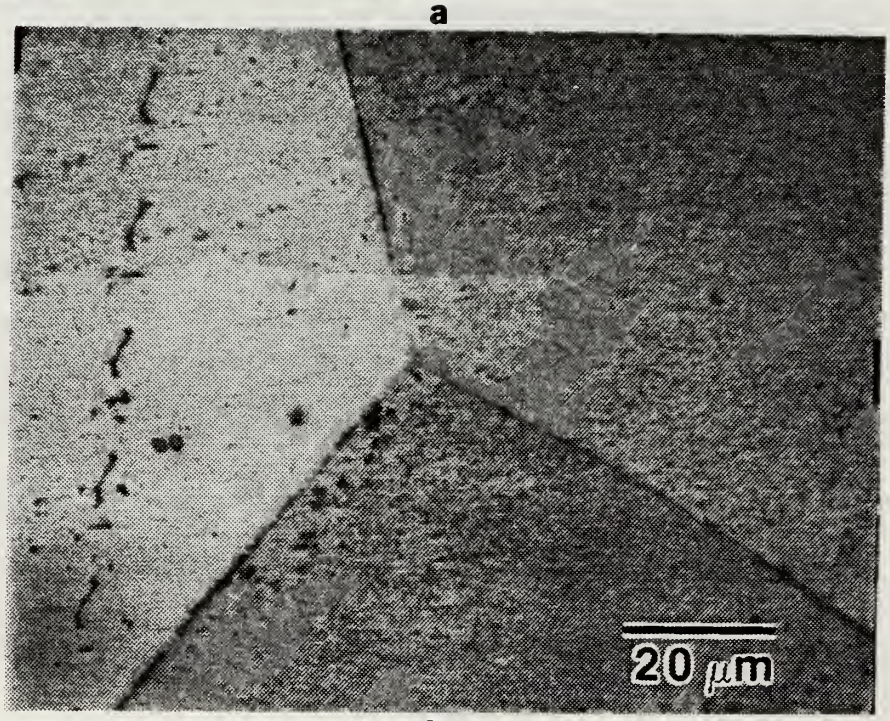

b

Figure 3.13 Optical Micrograph of Furnace Cooled VACROSIL-010(Mo) at (a) 50X and (b) 1000X Annealed 1 Hour at 1000°C.

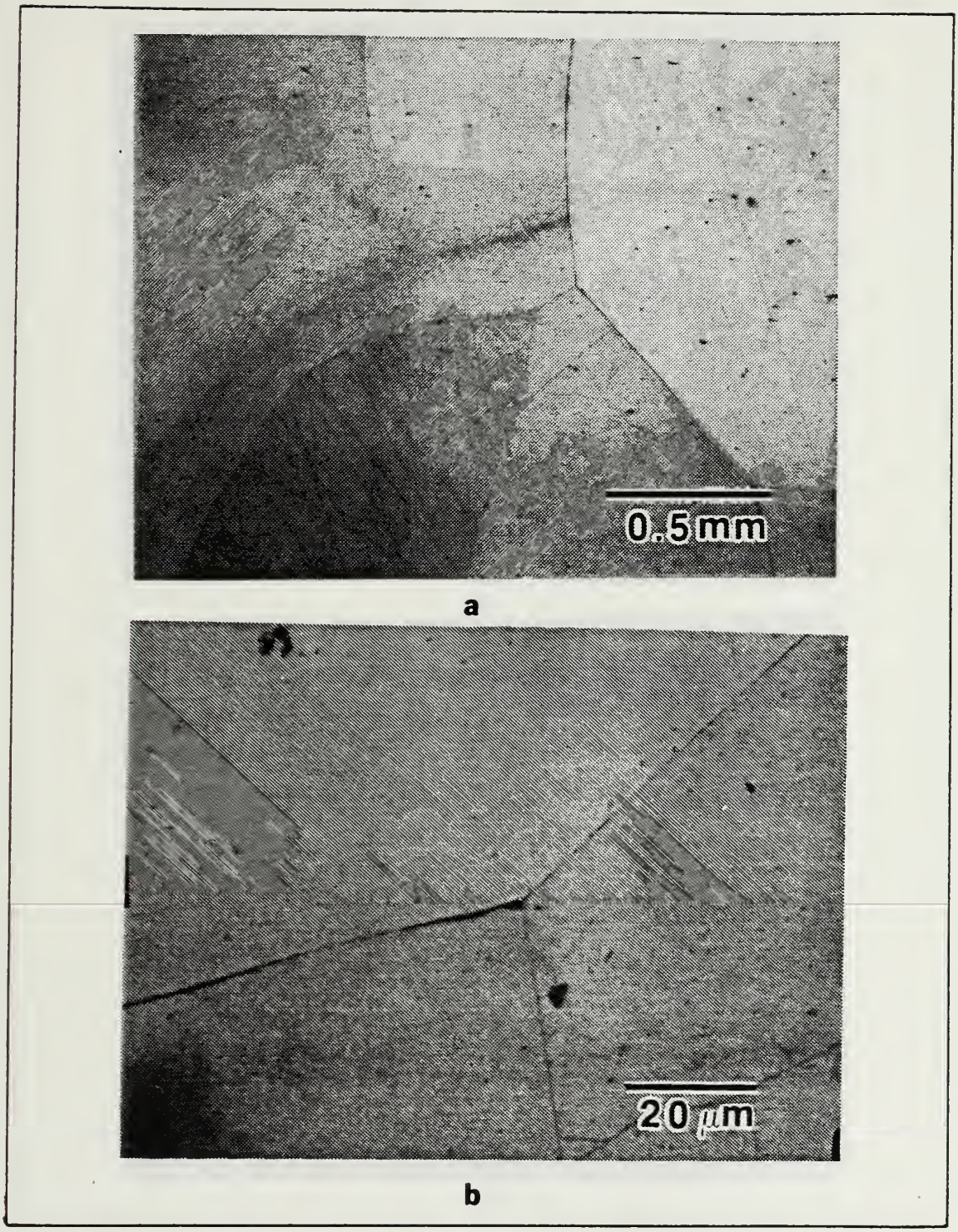

Figure 3.14 Optical Micrograph of Furnace Cooled VACROSIL-010(Mo) at (a) 50X and (b) 1000X Annealed 1 Hour at 1100°C.

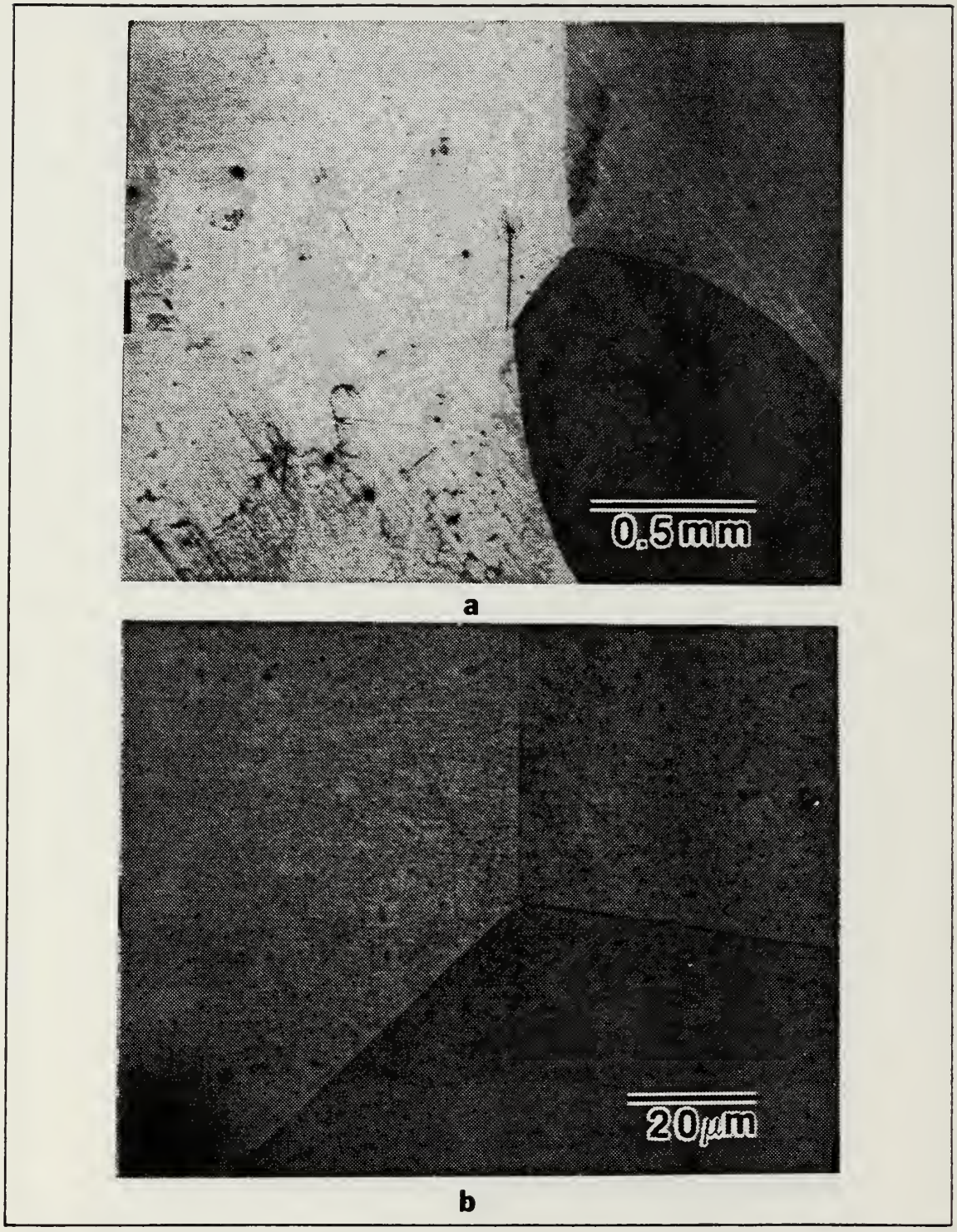

Figure 3.15 Optical Micrograph of Water Quenched VACROSIL-010(Mo) at (a) 50X and (b) 1000X Annealed 1 Hour at 800°C.

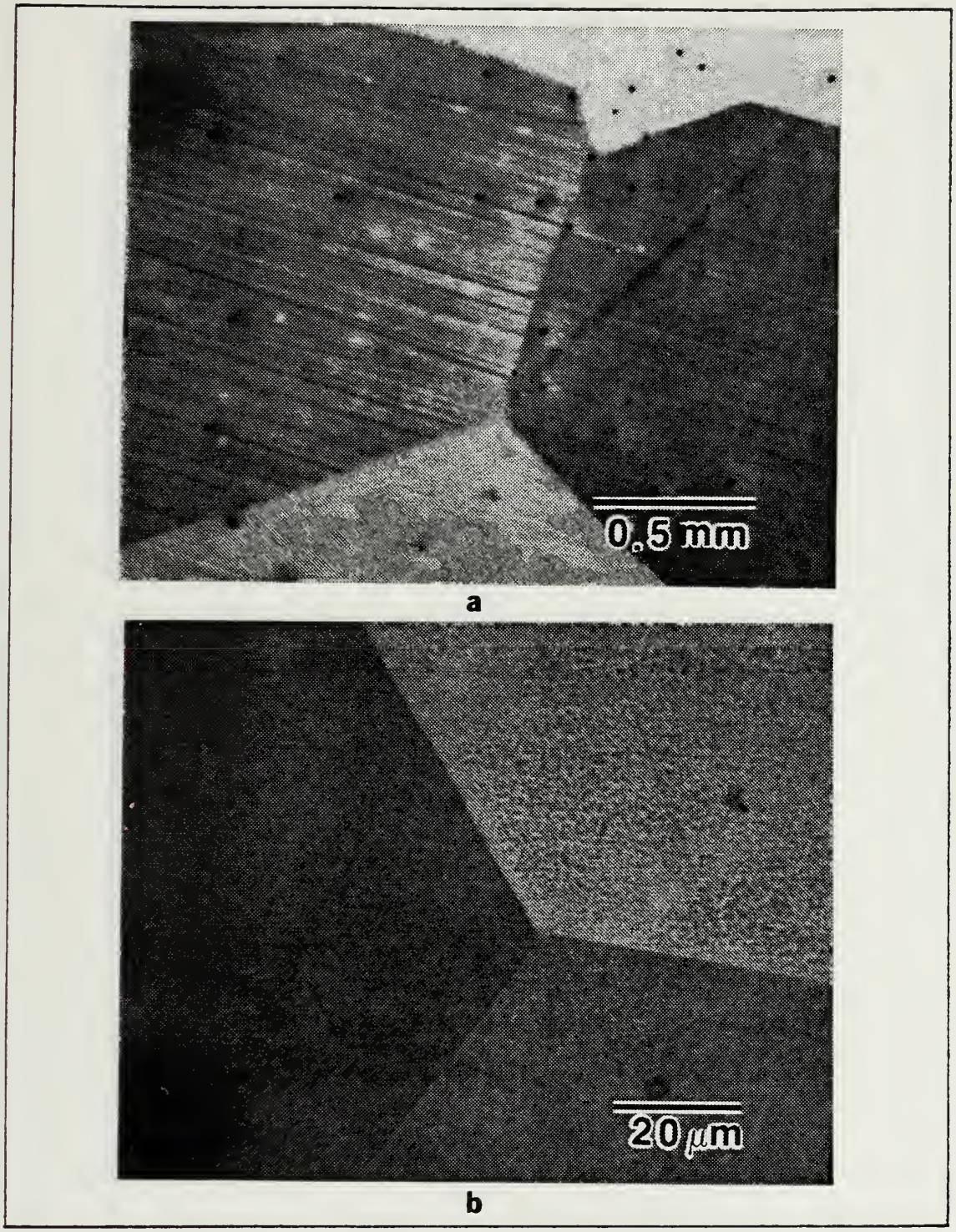

Figure 3.16 Optical Micrograph of Water Quenched VACROSIL-010(Mo) at (a) 50X and (b) 1000X Annealed 1 Hour at 900°C.

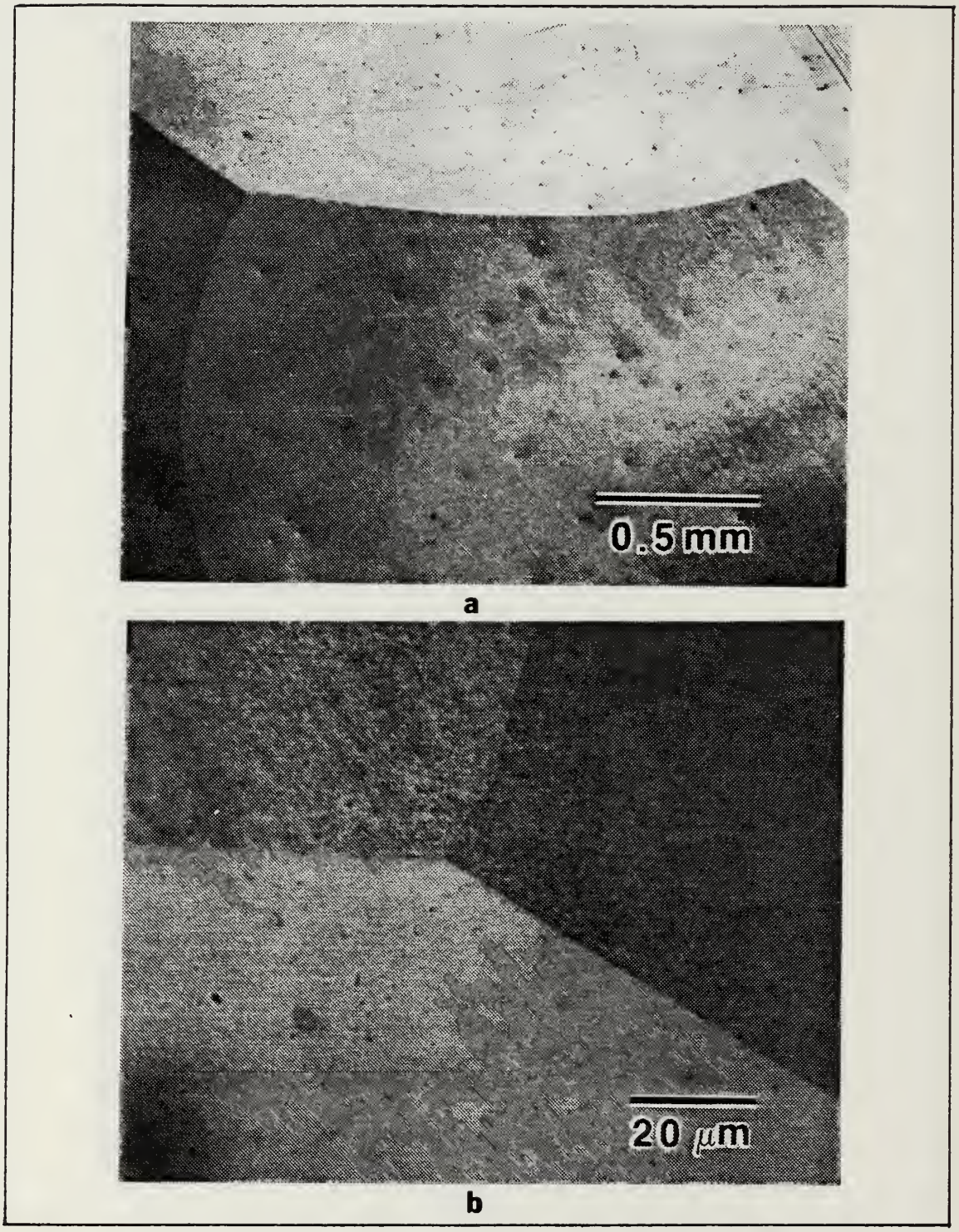

Figure 3.17 Optical Micrograph of Water Quenched VACROSIL-010(Mo) at (a) 50X and (b) 1000X Annealed 1 Hour at 1000°C.

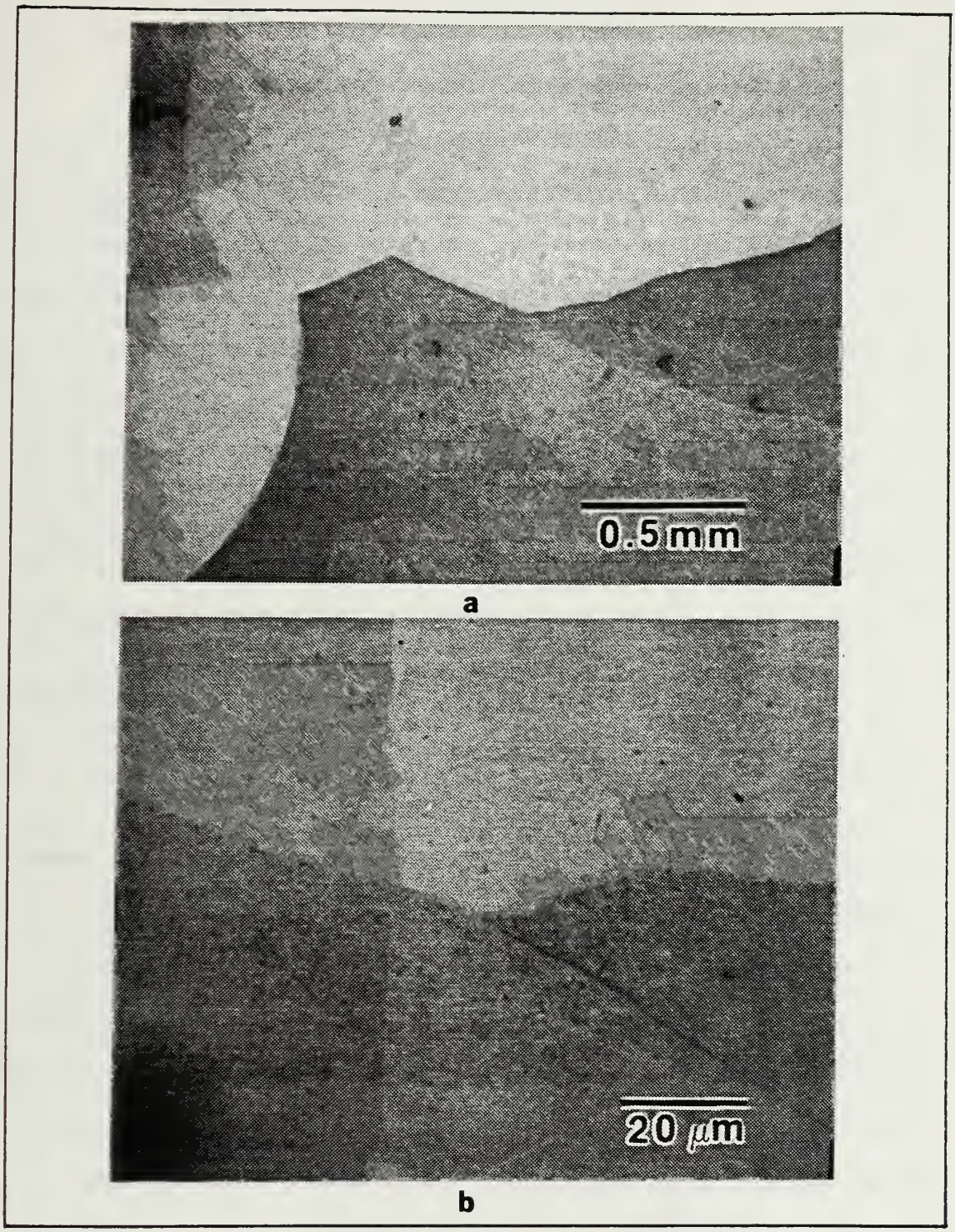

Figure 3.18 Optical Micrograph of Water Quenched VACROSIL-010(Mo) at (a) 50X and (b) 1000X Annealed 1 Hour at 1100°C.

After careful examination of the microstructures, the following scenario for this alloy is presented:

- At 1100°C, the material appears to be holding just above the nose of the(α + γ) two phase region, but in the α region, and upon furnace cooling, passes through the (α + γ) two phase region, where formation and then dissolution of the γ phase leads to the observed subgrain structure. However, the length of time that the alloy is in the two phase region is insufficient to allow complete formation of the γ phase. Subsequently, formation of an in termetallic second phase appears along the ferrite grain boundaries. Specimens quenched from 1100°C showed no evidence of a subgrain structure and little precipitation of an intermetallic phase along the grain boundaries. Quenching the material apparently retards the $\alpha \rightarrow \gamma$ diffusional reaction and χ phase formation.

- At 1000°C, it is not certain whether the alloy is within the (α + γ) or γ region based on our optical microscopic observations. However, precipitation of the χ phase again is evident upon furnace cooling only (not evident in the water quenched specimens), and no subgrain structures in the ferrite was evident.

- At 800°C and 900°C it can be safely assumed that the alloy is below the gamma loop. Again, there is some intermetallic phase (χ) precipitation along the grain boundaries in the furnace cooled specimens.

In summary, based on optical microscopic examination, it is not possible to discern a marked correlation between microstructure and damping capacity of the alloy. A second phase **does** appear to be decorating the grain boundaries of the furnace cooled specimens, but clearly this is not causing a detrimental effect on damping.

C. X-RAY DIFFRACTION RESULTS

As stated previously, the chromium content of the VACROSIL-010(Mo) experimental alloy was measured at 11.28%, placing it in close proximity to the (α + γ) two phase region. The molybdenum (Mo) content of VACROSIL-010(Mo) was measured at 2.45 weight %. Both Cr and Mo are bcc structures and ferrite stabilizers. Analysis of X-ray diffraction results revealed essentially a bcc structure throughout. There was no indication of any lattice distortion or additional peaks which might correspond to the formation of any additional phases. The mass densities (ρ) for each heat treatment are provided in Table 5.

TABLE 4

LATTICE PARAMETERS FOR EACH HEAT TREATMENT CONDITION OF VACROSIL-010

ANNEALING TEMPERATURE (°C)	LATTICE PARAMETER (ANGSTROMS)	
	WATER QUENCH	FURNACE COOL
800	2.8778	2.8784
900	2.8756	2.8765
1000	2.8743	2.8748
1100	2.8769	2.8768

TABLE 5

DENSITY VARIATION IN VACROSIL-010 WITH HEAT TREATMENT

ANNEALING TEMPERATURE (°C)	DENSITY (LBS/IN³) WATER QUENCH	FURNACE COOL
800	.278449	.280216
900	.281525	.279527
1000	.280101	.281023
1100	.283073	.282784

D. MECHANICAL PROPERTIES OF VACROSIL-010

The mechanical and electomagnetic characteristics of VACROSIL-010 are presented (see Table 6) from the manufacturer's specifications.

TABLE 6

MECHANICAL AND ELECTROMAGNETIC CHARACTERISTICS OF VACROSIL-010 [Ref. 15:p. 3]

Ultimate tensile strength	450N/mm²	65,264.34psi
Elastic limit (yield point) at 0.2% strain	320N/mm²	46,410.21psi
Density	7.47g/cm³	0.24219 lb/in³
Young's Modulus	175KN/mm²	25.38 X 10^6 psi
Electrical Conductivity	0.96 X 10^6 s/m	0.96 X 10^6 mho/m
Relative permeability	μ_r	300

Figures 3.19 and 3.20 are composite stress-strain diagrams for the water quenched and furnace cooled tensile specimens of the presently investigated VACROSIL-010(Mo). Hardness and elongation data are provided in Table 7. These results agree with handbook values for ferritic

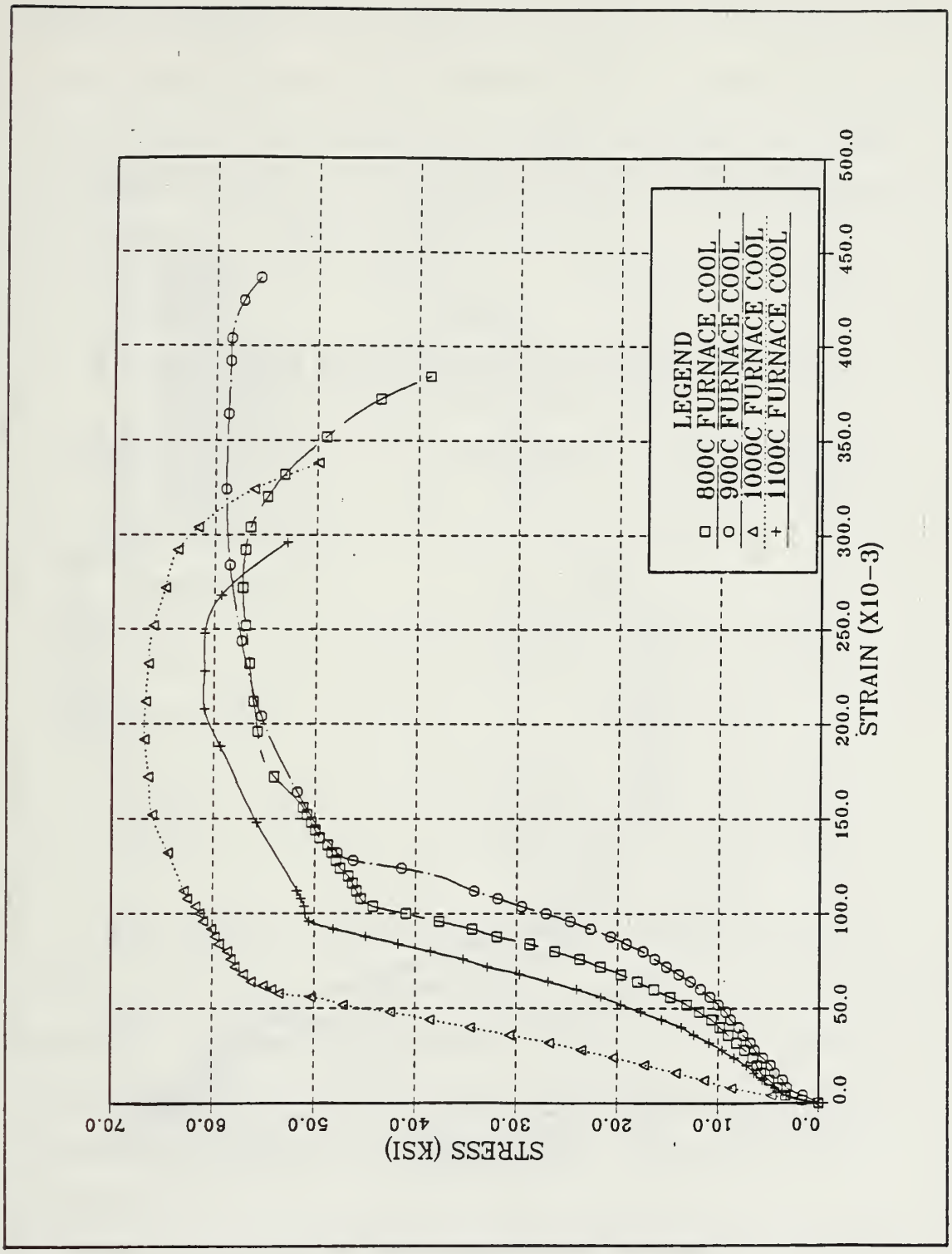

Figure 3.19 Stress-Strain Curves for Fractured Furnace Cooled Tensile Specimens.

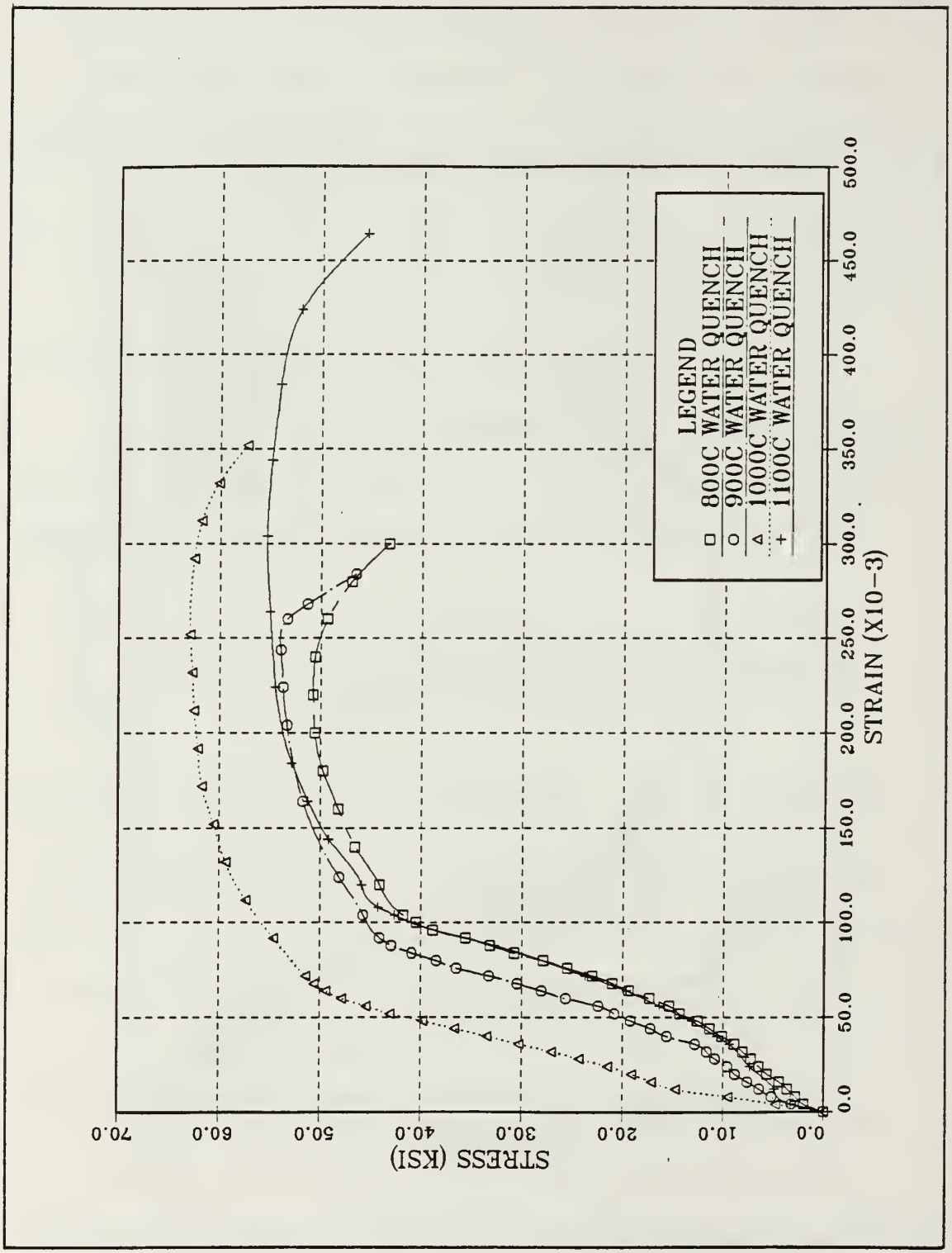

Figure 3.20 Stress-Strain Curves for Fractured Water Quenched Tensile Specimens.

stainless steels. No appreciable change in hardness associated with annealing temperature is noted in either the furnace cooled or water quenched samples. A slight increase in ductility is noted with annealing temperature in the water quenched samples.

TABLE 7

HARDNESS AND ELONGATION DATA FROM TENSILE TESTS OF VACROSIL-010

HEAT TREATMENT (°C)	HARDNESS (R_B)	ELONGATION (%)
WATER QUENCH		
800	80.73	29
900	82.375	24
1000	80.725	32
1100	80.64	43
FURNACE COOL		
800	85.69	25
900	83.14	28
1000	83.625	26
1100	87.07	24

The Appendix contains scanning electron microscope (SEM) photographs of the fracture surfaces of each tensile specimen. It can be seen that ductile rupture characteristics increase with annealing temperature in the water quenched specimens. Inclusions were evident in all samples.

The most significant aspect of the tensile loading data (Figures 3.19 and 3.20) occurs in the elastic region of the stress-strain curves, where a distinct region of

nonlinear elasticity was observed in all samples with the exception of the 1000°C heat treatment (both WQ and FC). A more defined view of this is presented in Figures 3.21 and 3.22. The absence of this feature in the 1000°C samples correlates with the lower damping capacity noted earlier for this heat treatment. In addition, a marked increase in Young's Modulus is noted, in contrast to the other heat treatments (the modulus of the 1000°C sample is approximately 16% - 21% greater in WQ specimens and 33% - 37% greater in FC specimens than in samples from the other annealing temperatures).

Cyclic hysteresis tests were also conducted for 900°C and 1100°C furnace cooled specimens, (loading to and unloading from 100, 250, and 500 lbs. for each specimen) as shown in Figures 3.23 and 3.24, respectively. The loading is normalized for reduced cross sectional area. Unloading is typified by an elasticity such that subsequent loading forms a narrow hysteresis loop. Each of these loops is characteristic of a hysteresis response which is pseudoelastic in nature. Pseudoelasticity is well known to occur in association with martensitic transformations and with the reversible movement of twin boundaries [Ref. 32]. These loops reflect the same sort of loading response indicated by the regions of nonlinear elasticity noted in Figures 3.21 and 3.22. What appears to be occuring is a

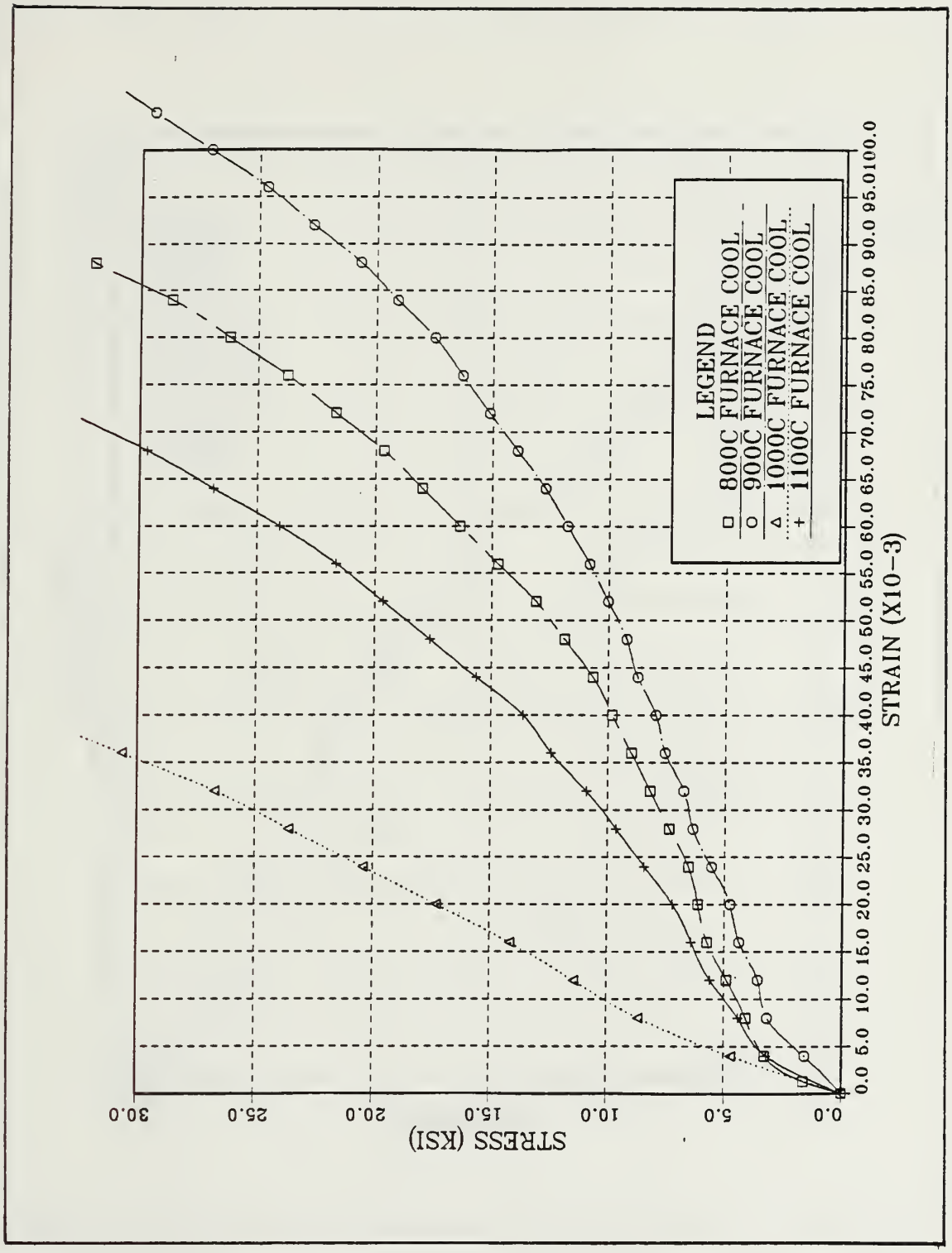

Figure 3.21 Nonlinear region of Furnace Cooled Stress-Strain Curves.

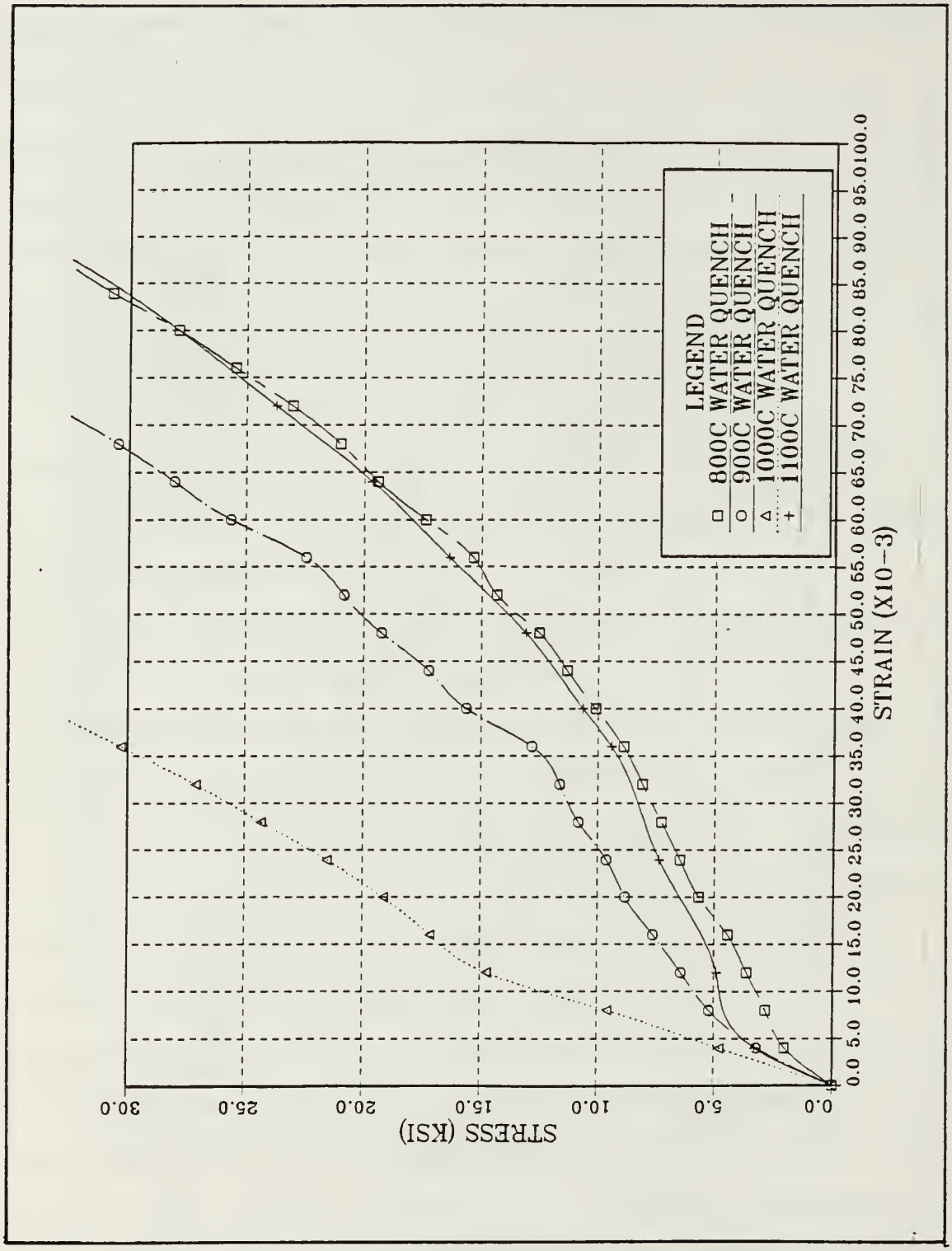

Figure 3.22 Nonlinear region of Water Quenched Stress-Strain Curves.

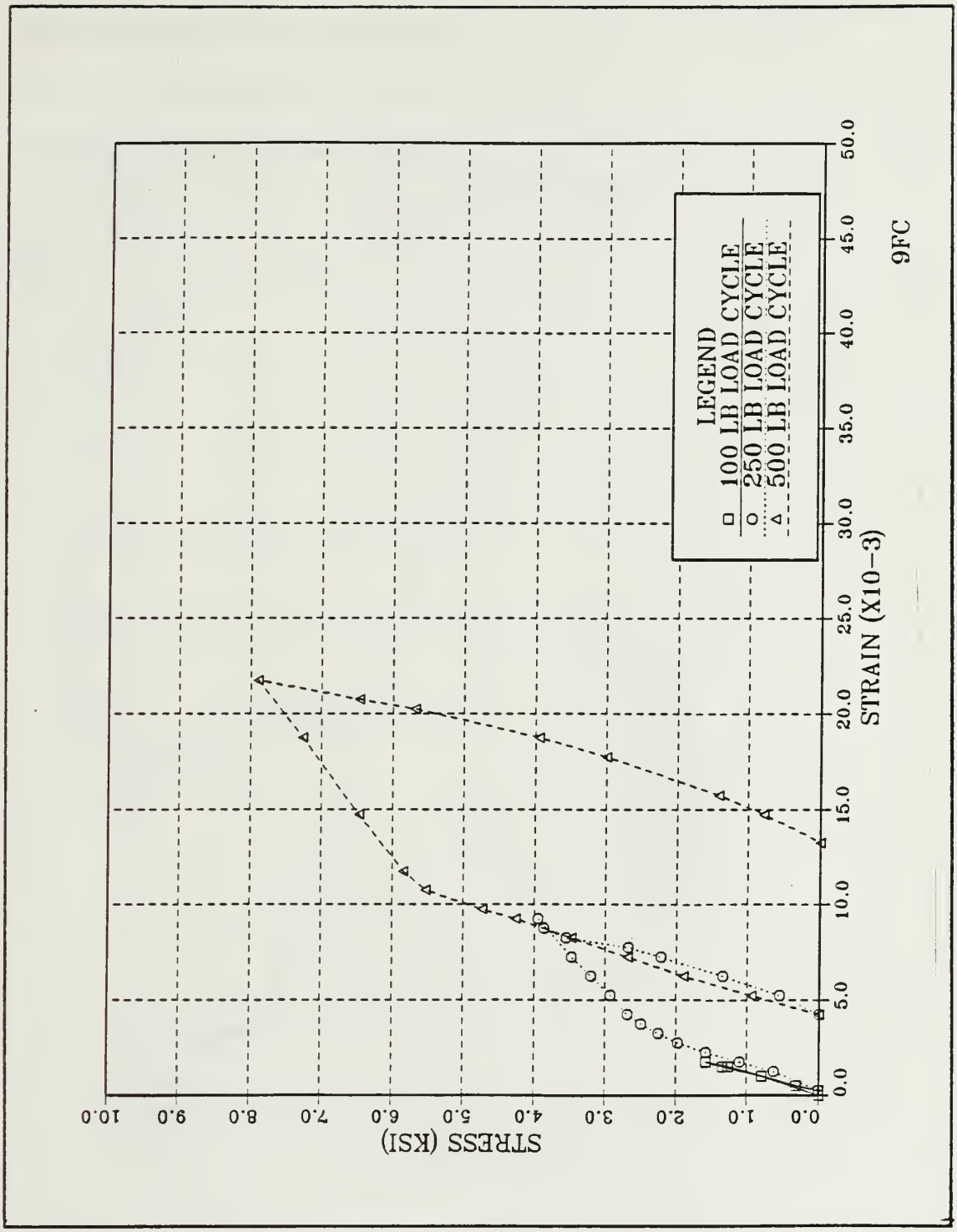

Figure 3.23 Hysteresis Response of 900°C Furnace Cooled Tensile Specimen of VACROSIL-010(Mo) Cyclically-Loaded in Pseudoelastic Region.

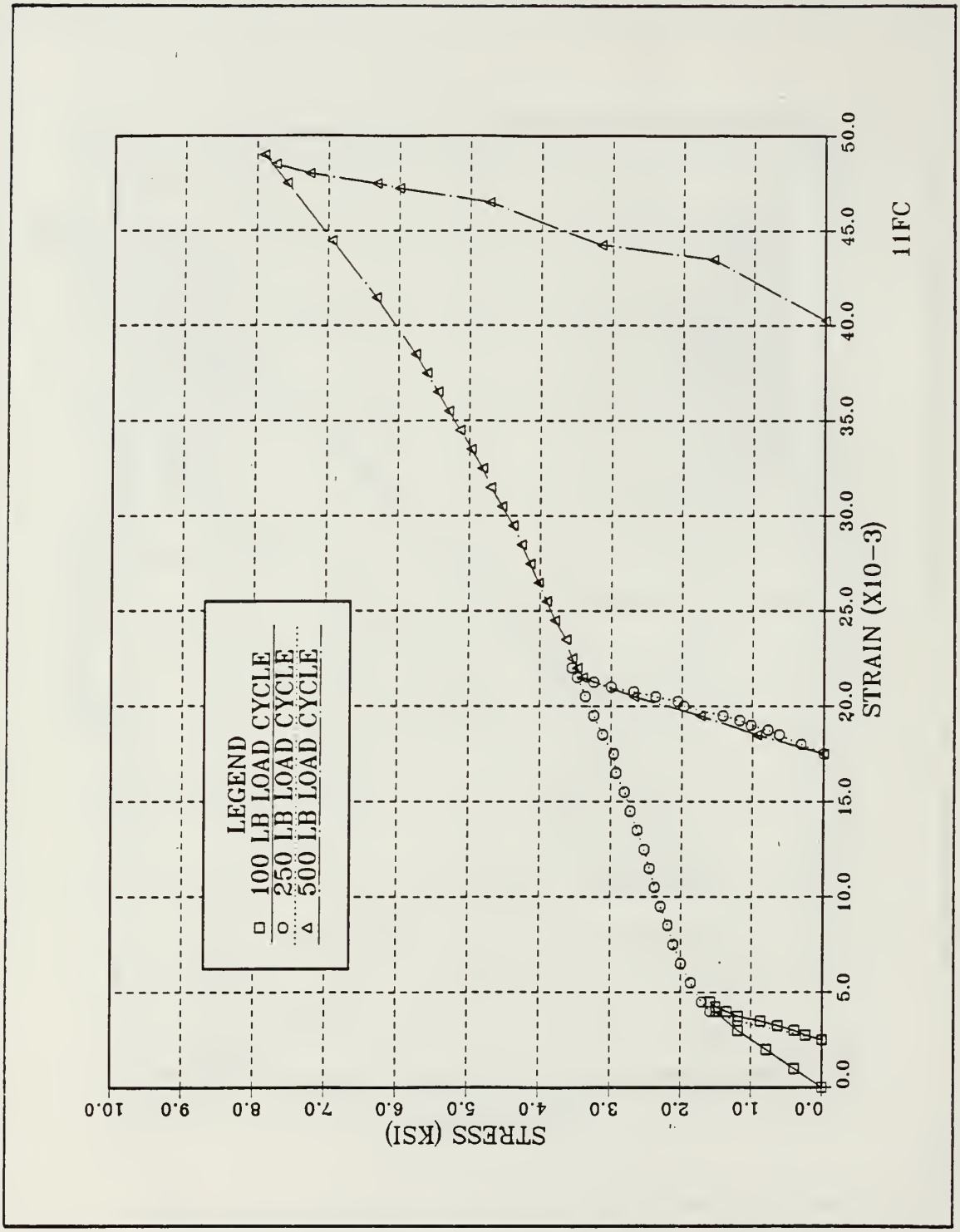

Figure 3.24 Hysteresis Response of 1100°C Furnace Cooled Tensile Specimen of VACROSIL-010(Mo) Cyclically-Loaded in Pseudoelastic Region.

manifestation of pseudoelasticity due to the magneto-mechanical response of the domain structure. The significance of the lack of a pseudoelastic effect in the 1000°C specimens can not be overlooked.

IV. CONCLUSIONS AND RECOMMENDATIONS

A. CONCLUSIONS

It has been demonstrated that VACROSIL-010(Mo) has quite high damping capacity under forced flexural vibration after it has been annealed at temperatures above 1100°C and allowed to cool at a rate which prevents the buildup of internal stress in the material. Development of high damping in VACROSIL-010(Mo) requires a minimum residual stress state within the material.

It has also been demonstrated that activation of the ferromagnetic damping mechanism is extremely stress (strain) dependent, exhibiting a saturation effect at a certain critical stress. Beyond this point, it will experience a slight decrease in damping with applied stress below the yield point.

On the optical microscopic level of examination, no observable effects were noted in the microstructure which may be correlated with variations in damping capacity.

During tensile testing, a pseudoelastic effect was noted in the stress-strain curves for all heat treatments except 1000°C. This indicates the possibility of differences in the microstructure not observable at the optical level of observation.

B. RECOMMENDATIONS

The following recommendations are proposed for further research and study on VACROSIL-010(Mo).

a. Determination of microstructural features at a more sophisticated level of observation.

b. More quantitative determination of the effect of cooling rate on the damping capacity of VACROSIL-010.

c. Determination of phase changes occuring upon heating/cooling, such as via dilatometry.

d. Ultilization of heating and cooling stages in the transmission electron microscope (TEM) to observe effects on magnetic domains above and below the Curie temperatures.

e. Study the effects of prolonged vibration on the damping of VACROSIL-010 specimens.

APPENDIX

FRACTURE SURFACE MICROGRAPHS FOR VACROSIL-010(Mo)

This appendix contains scanning electron microscopic (SEM) photographs of the fracture surfaces of tensile specimens corresponding to 1 hour annealing at 800°C, 900°C, 1000°C and 1100°C (furnace cooled or water quenched).

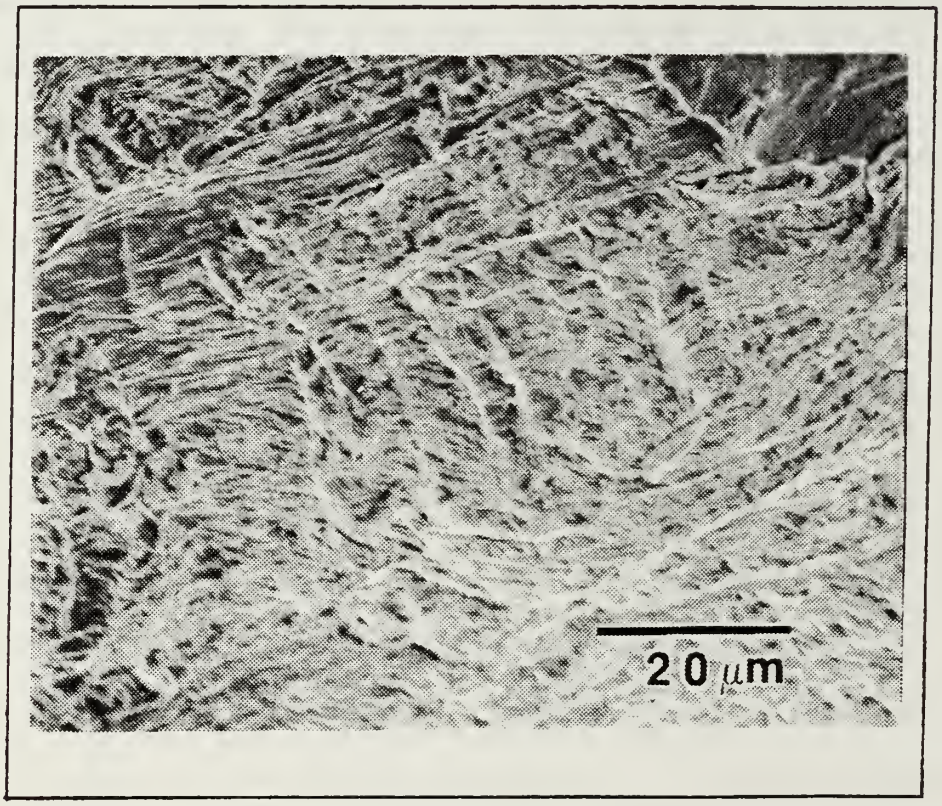

Figure A.1 Fracture Surface for Tensile Specimen of Water Quenched VACROSIL-010(Mo) annealed 1 hour at 800°C, (1.22KX).

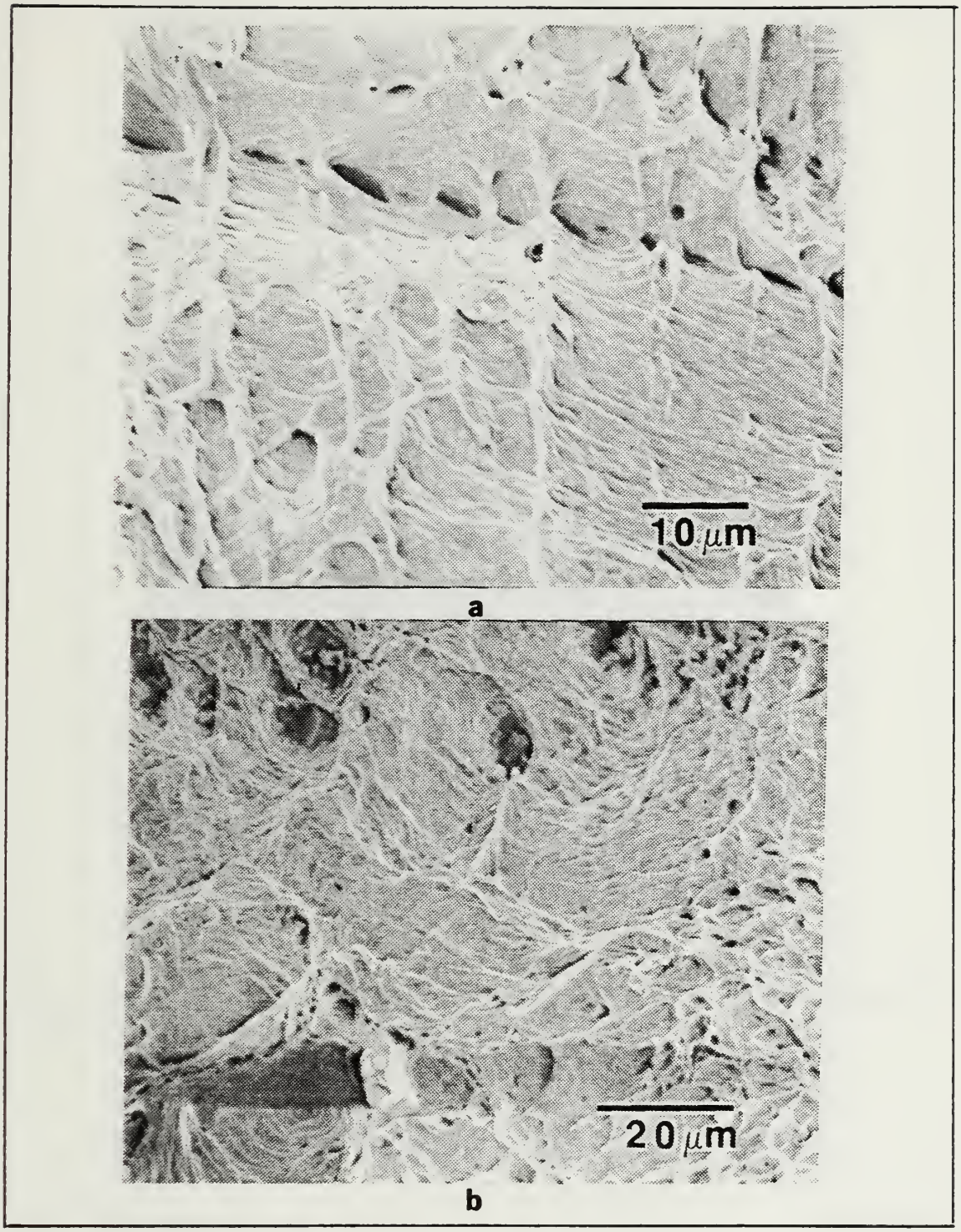

Figure A.2 Fracture Surface for Tensile Specimen of Water Quenched VACROSIL-010(Mo) annealed 1 hour at (a) 900°C (1.60KX) abd (b) 1000°C (1.03KX).

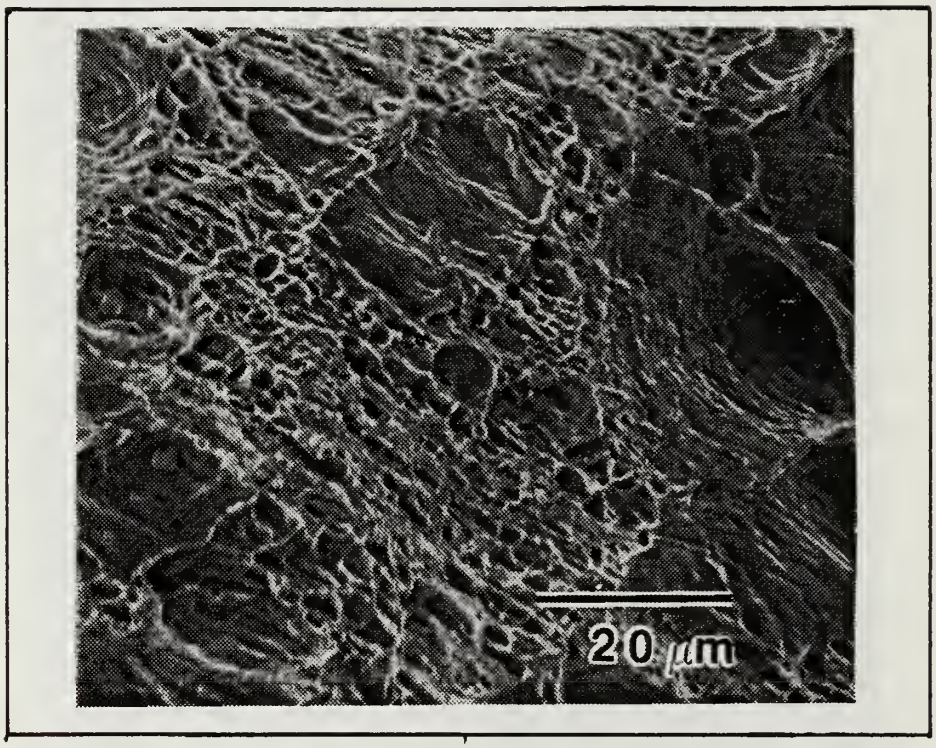

Figure A.3 Fracture Surface for Tensile Specimen of Water Quenched VACROSIL-010(Mo) annealed 1 hour at 1100°C (1.23KX).

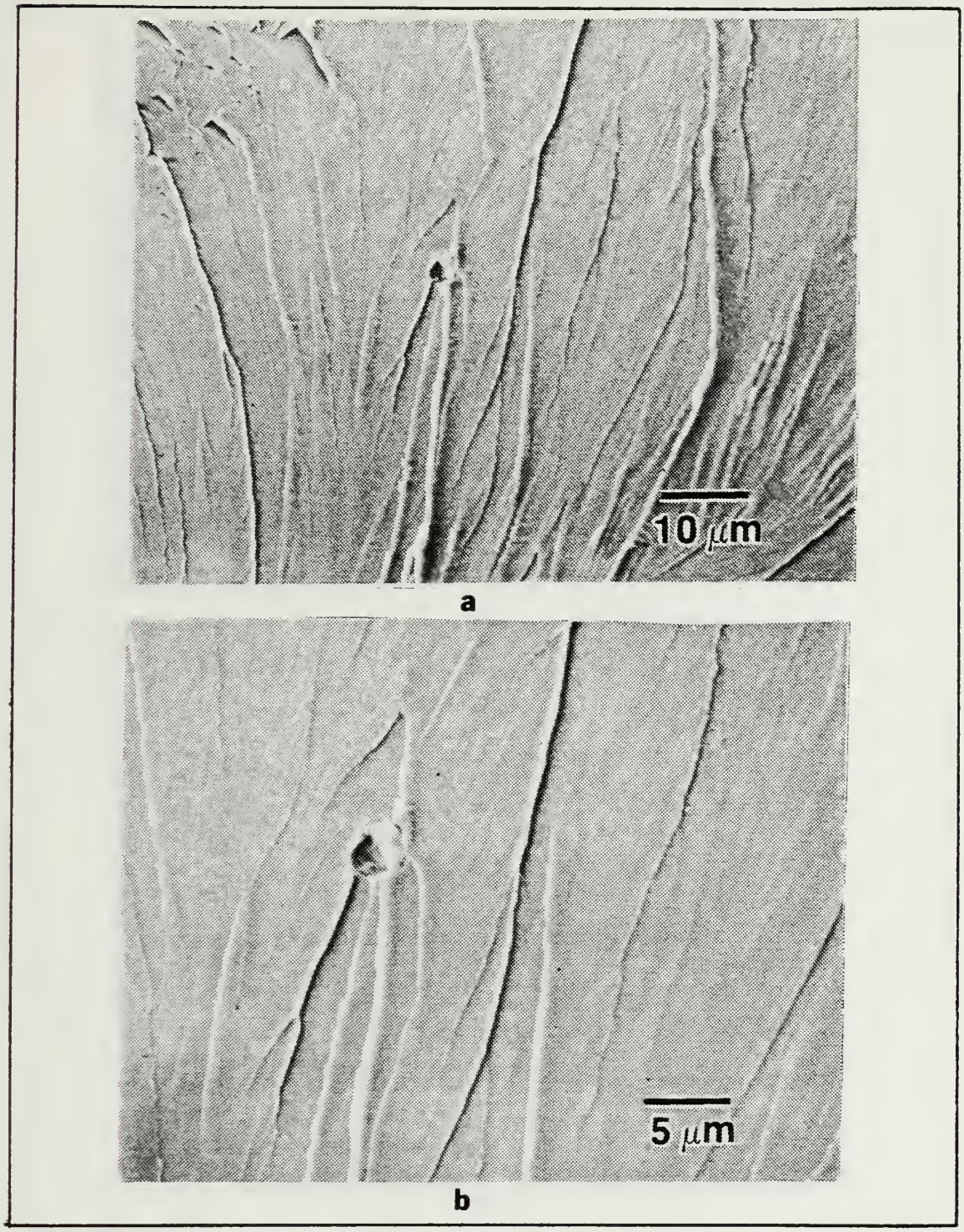

Figure A.4 Fracture Surface for Tensile Specimen of Furnace Cooled VACROSIL-010(Mo) annealed 1 hour at 800°C (a) 1.32KX and (b) 2.62KX

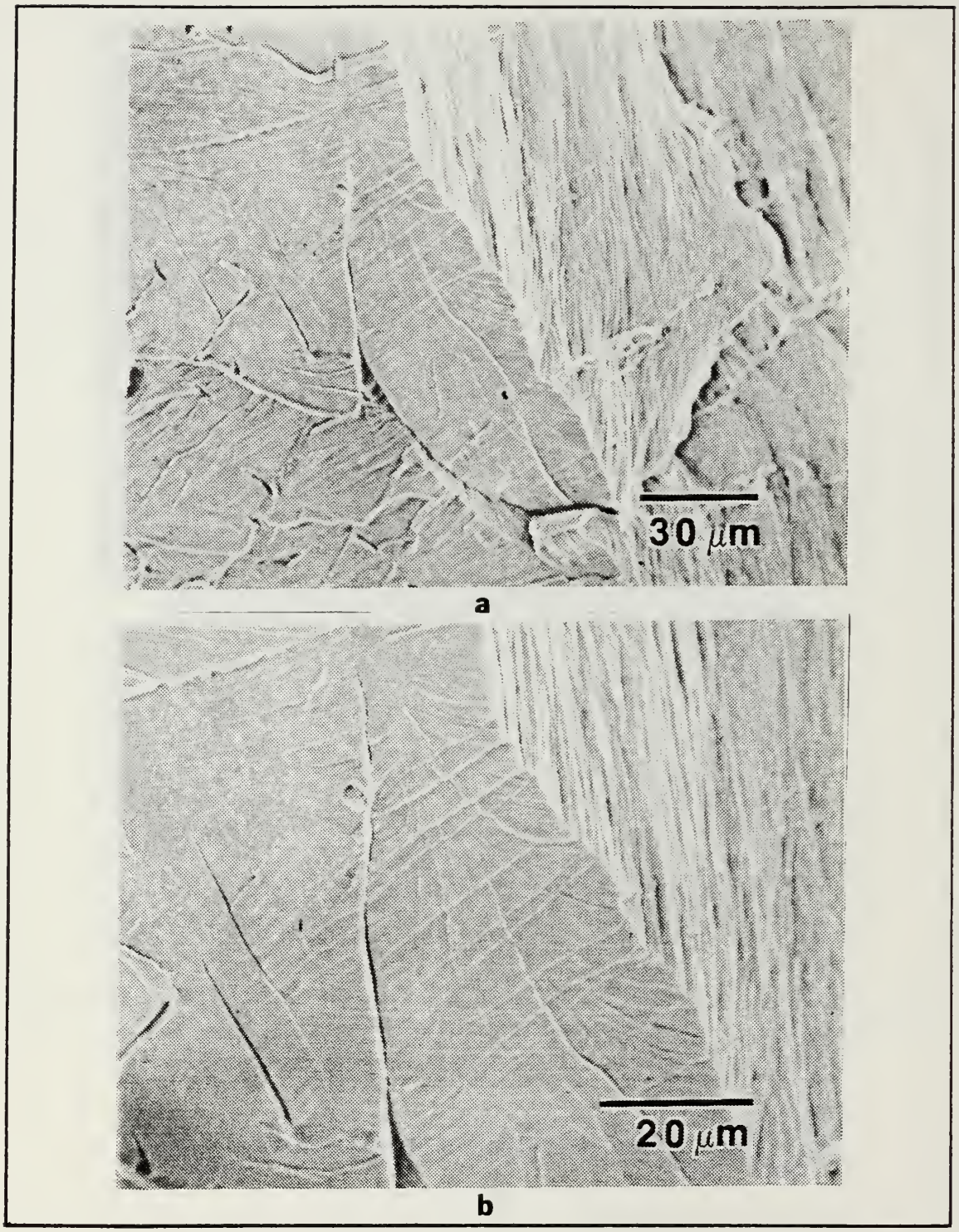

Figure A.5 Fracture Surface for Tensile Specimen of Furnace Cooled VACROSIL-010(Mo) annealed 1 hour at 900°C (a) 596X and (b) 1.15KX.

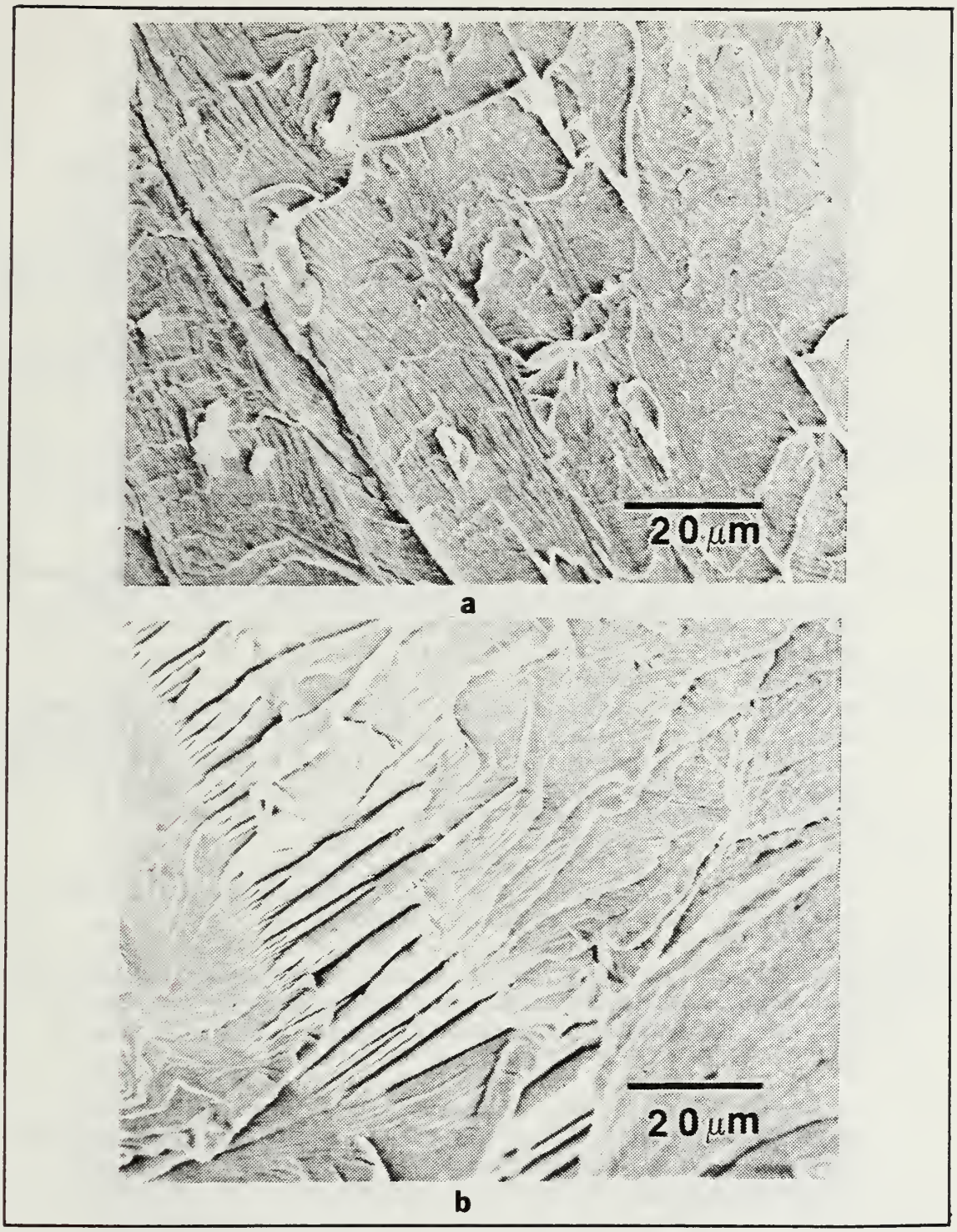

Figure A.6 Fracture Surface for Tensile Specimen of Furnace Cooled VACROSIL-010(Mo) annealed 1 hour at (a) 1000°C (1.02KX) and (b) 1100°C (1.02KX).

LIST OF REFERENCES

1. Schetky, L.M. and Perkins, J., "The 'Quiet' Alloys," Machine Design, pp. 202-206, 6 April 1978.

2. Naval Research Laboratory Internal Report, Acoustic Damping Materials, A Review, by R.A. Meussner and B.B. Rath, November 1982.

3. de Batist, R., "High Damping Materials: Mechanisms and Applications," Journal de Physique, Vol. 44, pp. C9-39-C9-50, December 1983.

4. Granato, A. and Lucke, K., "Theory of Mechanical Damping Due to Dislocations," Journal of Applied Physics, Vol. 17, No. 6, pp. 583-593, June 1956.

5. Dew, D.D., Strain Dependent Damping Characteristics of a High Damping Manganese-Copper Alloy, M.E. Thesis, Naval Postgraduate School, Monterey, California, September 1986.

6. Reskusich, J., Cyclic Strain Amplitude and Heat Treatment Effects on the High Damping Behavior of Incramute Alloy Under Random Vibration Loading in the 50-1000 Hz Frequency Range, M.E. Thesis, Naval Postgraduate School, Monterey, California, September 1986.

7. Cochardt, A.W., "The Origin of Damping in High-Strength Ferromagnetic Alloys," Transactions of the ASME, Vol. 75, pp. 196-200, 1953.

8. Schilling, J.W. and Houze, G.L., "Magnetic Properties and Domain Structure in Grain-Oriented 3% Si-Fe," IEEE Transactions on Magnetics, Vol. MAG-10, No. 2, pp. 195-222, June 1974.

9. Willertz, L.E., "Magnetomechanical Damping Properties of AISI 403 Stainless Steel with Applied Static Torsional and Axial Stresses," Journal of Testing and Evaluation, JTEVA, Vol. 2, No. 6, pp. 478-482, November 1974.

10. Suzuki, K., Fijita, T., and Haseb, M., "Damping Capacity and Mechanical Properties of Sintered Fe-Cr-Mo High Damping Alloy," Powder Metallurgy, No. 4, pp. 205-211, 1977.

11. Masumoto, H., Sawaya, S., and Hinai, M., "On the Damping Capacity of Fe-Cr Alloys," Journal of Japan Institute of Metal, (in Japanese), 43, pp. 409-413, 197).

12. Masumoto, H., Sawaya, S., and Hinai, M., "Damping Characteristics of 'Gentalloy' in the Fe-Mo System," Transactions of the Japan Institute of Metals, Vol. 22, No. 9, pp. 607-613, 1981.

13. Masumoto, H., Sawaya, S., and Hinai, M., "Damping Capacity and Pitting Corrosion Resistance of Fe-Mo-Cr Alloys," Transactions of the Japan Institute of Metals, Vol. 25, No. 12, pp. 891-899, 1984.

14. Schneider, W., Schrey, P., Hausch, G., and Torok, E., "Damping Capacity of Fe-Cr and Fe-Cr Based High Damping Alloys," Journal De Physique, Colloque C5, Supplement au n 10, Tome 42, pp. C5-C35, October 1981.

15. Naval Underwater Systems Center Report TD 6927, A Technical Update on Damped Vacrosil-010, by R.G. Kasper, 19 September 1983.

16. Kawabe, H. and Kuwahara, K., "Effects of Material Damping on the Suppression of Mechanical Vibrations," Bulletin of the JSPE, Vol. 14, No. 1, pp. 31-36, March 1980.

17. Kawabe, H. and Kuwahara, K., "A Consideration of the Strain Amplitude-Dependent Damping and Modulus in Ferromagnetic Metals," Transactions of the Japan Institute of Metals, Vol. 22, No. 5, pp. 301-308, 1981.

18. Amano, K., Sahashi, M., Tokoro, H., and Nakagawa, M., "High Damping Characteristics of Fe-Cr-Al Alloys Associated with their Magnetic Properties," Proceedings of the 6th International Conference on Internal Friction and Ultrasonic Attenuation in Solids, Ed. R.R. Hasiguti and N. Mikoshiba, University of Tokyo Press, pp. 763-767, 4-7 July 1977.

19. Kawabe, H. and Kuwahara, K., "Damping - and Modulus-Measurement of High-Damping Metal 'SIA' at Low Frequencies," Proceedings of the 6th International Conference on Internal Friction and Ultrasonic Attenuation in Solids, Ed. R.R. Hasiguti and N. Mikoshiba, University of Tokyo Press, pp. 781-785, 4-7 July 1977.

20. Bert, C.W., "Material Damping: An Introductory Review of Mathematical Models, Measures, and Experimental Techniques," Journal of Sound and Vibration, Vol. 29, No. 2, pp. 129-153, 1973.

21. Thomson, W.T., Theory of Vibrations with Applications, Prentice-Hall, Inc., 1981.

22. Reed-Hill, R.E., Physical Metalurgical Principles, Brooks/Cole Engineering Div., 1973.

23. Bolt, Beranek, and Newman, Inc., Cambridge, Massachusetts, "Operations Manual for the Bolt, Beranek, and Newman, Inc., Resonant Dwell Apparatus," January 1973.

24. Kaufman, L., Kulin, S.A., and Neshe, P., "Internal Vibration Absorption in Potential Structural Materials," Shape Memory Effects in Alloys, Jeff Perkins, ed., Plenum Press, pp. 547-561, 1975.

25. DeGauque, J., Astie, B., and Kubin, L.P., "Evidence for the Interaction Between Magnetic Domain Walls and Dislocations in High-Purity Iron from Magnetomechanical Damping Experiments," Phys. Stat. Sol., Part A, Vol. 45, pp. 493-501, 1978.

26. Askeland, D.R., The Science and Engineering of Materials, Wadsworth, Inc., 1984.

27. Wolfenden, A., "Damping in Turbine Blade Alloys," Journal of Testing and Evaluation, JTEVA, Vol. 10, No. 1, pp. 17-20, January 1982.

28. Peckner, D. and Bernstein, I.M., Handbook of Stainless Steels, McGraw-Hill, Inc., 1977.

29. Metals Handbook, 8th ed., Vol. 8, American Society for Metals, 1973.

30. Grigor'ev, S.B. and Kudryashova, L.K., "Magnetoelastic Attenuation due to Rotation of Magnetization," Soviet Phys. Solid State, Vol. 17, No. 1, pp. 99-102, July 1975.

31. "Standard Methods of Tension Testing of Metallic Materials," ASTM E8-83, American Society for Testing and Materials, Vol. 03.01, pp. 130-150, 1983.

32. Otsuka, K. and Shimizum K., "Pseudoelasticity," Metals Forum, Vol. 4, No. 3, pp. 142-152, 1981.

INITIAL DISTRIBUTION LIST

		No. Copies
1.	Defense Technical Information Center Cameron Station Alexandria, Virginia 22304-6145	2
2.	Library, Code 0142 Naval Postgraduate School Monterey, California 93943-5002	2
3.	Department Chairman, Code 69Hy Department of Mechanical Engineering Naval Postgraduate School Monterey, California 93943-5000	1
4.	Professor A.J. Perkins, Code 69Ps Department of Mechanical Engineering Naval Postgraduate School Monterey, California 93943-5000	10
5.	Professor Y.S. Shin, Code 69Sg Department of Mechanical Engineering Naval Postgraduate School Monterey, California 93943-5000	1
6.	Lt. John F. O'Toole, Jr., USN 151 Westwood Drive East Greenwich, Rhode Island 02818	2
7.	Mr. Robert Hardy, Code 2803 David W. Taylor Naval Ship R & D Center Annapolis, Maryland 21402	5
8.	Ms. Cathy Wong, Code 2812 David W. Taylor Naval Ship R & D Center Annapolis, Maryland 21402	5